Dynamic Analysis of a Monopile Model

Jensen, Jakob Laigaard

Publication date:
1988

Document Version
Early version, also known as pre-print

INSTITUTTET FOR BYGNINGSTEKNIK

INSTITUTE OF BUILDING TECHNOLOGY AND STRUCTURAL ENGINEERING

AALBORG UNIVERSITETSCENTER · AUC · AALBORG · DANMARK

FRACTURE AND DYNAMICS

PAPER NO. 4

JAKOB LAIGAARD JENSEN

DYNAMIC ANALYSIS OF A MONOPILE MODEL

SEPTEMBER 1988

ISSN 0902-7513 R8824

CORRECTIONS

p 3, figure 1.3, text: mass 1 should be mass 2.

p 5, line 2-4 from the top should be changed to:

"The figure shows that the monopile is lightly damped. The first eigen frequency was about 1.10 Hz in the first main direction.".

p 15 , figure 3.4 and p 32, figure 4.4:

The figures do not show the lumped mass model of the monopile. The stiffness matrix of the lumped mass model was found from the flexibility matrix of a clamped beam.

p 22, (4.6): ω^2 should be ω_i^2.

p 23, after (4.11) should be added:

"where the weighted mode shape matrix is given by:

$$\Phi = \begin{pmatrix} \Phi_{11} & \Phi_{21} \\ \Phi_{12} & \Phi_{22} \end{pmatrix}$$

In the report the weighted mode shape matrix is also given by $\widetilde{\widetilde{\Phi}}$ when distinction from the unweighted mode shape matrix is necessary.".

p 26, (4.19): $=$ should be $\approx$.

p 30, (4.30): Φ_{t-2n} should be Φ_{2n} and Θ_{t-2n+1} should be Θ_{2n-1}.

p 31, (4.32): Θ_{2n} should be Θ_{2n-1} and after (4.32) should be added:

"and σ_a^2 is the variance of the white noise input.".

p 61, (3.14a) and (3.14b) should be (4.14a) and (4.14b).

Throughout the text: "spring blade" should be "leaf spring"

PREFACE

This report is the result of the experimental investigations of a monopile model performed at the Institute of Building Technology and Structural Engineering at the University of Aalborg.

The experimental work was carried out as a part of the project "Wave Induced Vibrations" which is supported by the Danish Technical Research Council.

The experiment was performed in cooperation with Mr. L. Pilegaard Hansen, M.Sc., Ph.D., and he and Mr. R. Brincker, M.Sc., Ph.D. have been helpful with advices in the analysis of the experimental results.

I want to express my sincere thanks to the staff in the laboratory, especially Mr. H. Andersen, who has come up with valuable suggestions for my project.

The drawings were made by Ingrid Christensen and her staff and Bente Jul Kjergaard has proofread the report.

Jakob Laigaard Jensen
Aalborg, September 1988.

DYNAMIC ANALYSIS OF A MONOPILE MODEL

Jakob Laigaard Jensen
University of Aalborg
Sohngaardsholmsvej 57, DK-9000 Aalborg
Denmark

ABSTRACT

The dynamic characteristics of a 4 meter high monopile model have been investigated. The monopile model had two concentrated masses and was described as a lightly damped two degrees of freedom system.

The model was excited by a shaker table. The interaction between the model and the shaker table had been examined and found acceptable. Sinusoidal signal and random noise have been used as excitation signals. Beside forced excitation, free vibration has also been used in the experiment.

The eigen frequencies and the damping ratios have been estimated. Different kinds of identification methods have been used. Identification using ARMA models was among those. The eigen frequencies were easily determined while the damping ratios were found to be rather uncertain. The most reliable damping estimates were determined from the free vibration and the estimated ARMA models. Some of the uncertainties and deviations could be explained by insufficient frequency resolution in the FFT analysis. Finally, mode shapes and transfer functions were estimated and compared with theory. A good agreement was found.

CONTENTS

SYMBOLS

a	acceleration vector
a_t	white noise in the discrete time domaine
A	cross section
$\overline{A}$	amplitude vector
ARMA(2n.2n-1)	autoregressive moving average model of order (2n,2n-1)
BW	effective bandwidth
$\overline{\overline{C}}$	damping matrix
b	index for the base
c_{cr}	critical damping coefficient
dt	sampling interval in seconds
df	frequency interval in Hz
d	index for damped motion
D_{ij}	dynamic amplification factor
E	linear elasticity coefficient
f	frequency in Hz
f_i	eigen frequency or discrete frequency
f_s	sampling frequency
$\overline{f}$	force vector
$\overline{\overline{h}}$	impulse response function matrix
$\overline{\overline{H}}$	frequency response function or transfer function matrix
$\overline{G}$	one sided discrete amplitude spectrum vector
$\overline{\overline{K}}$	stiffness matrix
L	length
m	mass per unit length
m_{ii}	modal mass of mode i
M_i	concentrated or lumped mass
$\overline{\overline{M}}$	mass matrix
n	number of averages

N	number of sampled means
p	periodic noise
p_c	cylinder force
$\overline{\overline{P}}$	phase response function matrix
RSS	residual sum of squares
$\overline{\overline{r}}$	correlation function matrix
$\overline{\overline{S}}$	one sided spectral density matrix
S_0	constant spectral density
t	time
t_i	discrete time
T	periode or time duration
T	transposed vector or matrix
$\overline{v}$	vertical displacement vector
x_b	horizontal base displacement
$\overline{u}$	horisontal displacement vector
w	white noise
α	constant
β	constant
δ	logarithmic decrement
γ	coherence function
ϵ	strain
ζ	damping ratio
θ	rotation or angle
λ	eigen value
π	pi
ρ	density
σ	stress
ω	frequency (rad/sec)
Δ	difference

Γ	variation coefficient
Θ	moving average parameter
Σ	summation
$\overline{\overline{\Phi}}$	mode shape matrix
Φ	autoregressive parameter or phase angel
$Re[]$	real part of complex number
$Im[]$	imaginary part of complex number
$\dot{}$	differentiation with respect to time
D	difference operator in the discrete time domain
$\|\|$	absolute value

Small letter cases refer to signal in time domaine. Large letter cases refer to signal in frequency domaine.

1 INTRODUCTION

The purpose of the experiment has primarily been to get some practical experience in testing and analysing a vibrating structure. The analysis has mainly been carried out from a system identification point of view.

A monopile with two concentrated masses was chosen as a model, see figure 1.1. First of all because it was a simple system to test and to analyse. Secondly, it was of importance that the system had some resemblance with the type of offshore construction called a monopile or a monotower. Thirdly, because the lowest eigen frequencies of the model had the same magnitude as the eigen frequencies of typical marine structures.

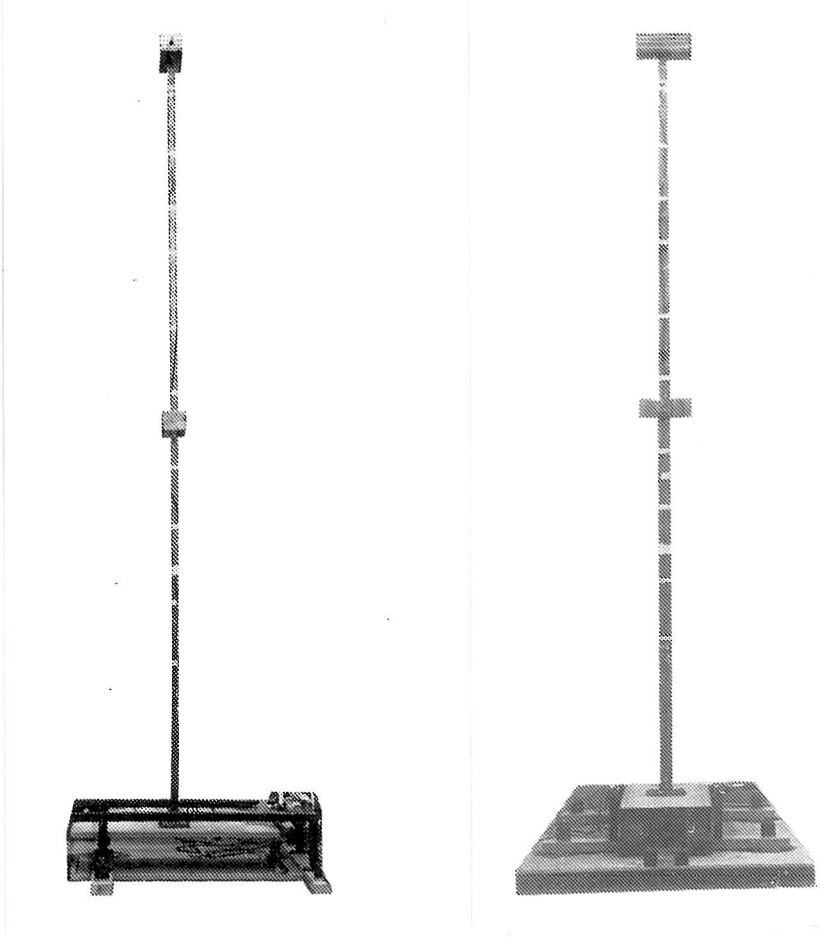

Figure 1.1. The monopile model and the excitation system.

The monopile model was made as a 4 meter high box profile (70-40-4 mm) with the two masses of approximately 25 kg, see figure 1.3. The monopile model was welded to a plate which was bolted to the base.

The monopile was excited due to horizontal movement of the base. The movement was created by a hydraulic cylinder, Schenck, type Pl 63H connected to a control system. The excitation system is shown in figure 1.2. The excitation was only made in one horizontal direction called the first main axis. The eigen modes in this direction is labelled the first, the second, the third etc. eigen modes. The eigen modes of the monopile model in the direction of the second main axis had only minor importance. The second main axis was defined as orthogonal axis in the plane of the base.

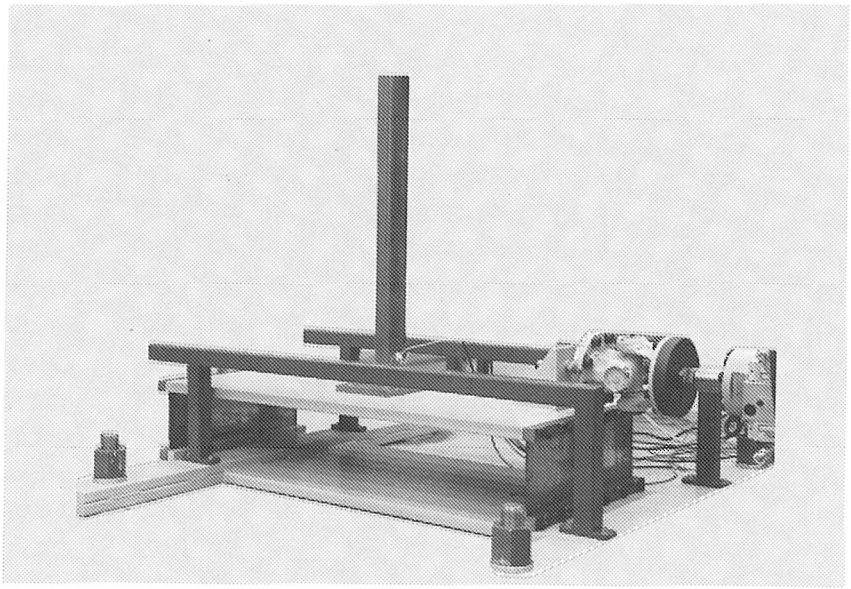

Figure 1.2. Excitation system of the base.

The shaker table system was chosen because of several reasons. First of all because this kind of excitation removes the problem of getting a proper force excitation with no constrained displacements. Secondly because it is difficult to place a force excitation at a height of 4 meter. Although it might be a problem with the shaker table that the model interacts with the base movement. Furthermore, some vibration of second order might be introduced, because the base does not move completely horizontally. This potential interaction problem has been investigated as a part of the experiment, see chapter 3.

The base excitation was given by the control system of the cylinder. The control system provided a sinusoidal shaped signal controlled by a given amplitude and frequency. As another input signal the control system could be given any signal from an external source. In the experiment the noise source from a HP3582A Spectrum Analyzer was used. This was able to give white noise as well as periodic noise. Besides, these kind of excitations a free vibration caused by a forced displacement was used.

The base displacement were measured by a displacement transducer with an amplifier, type HBM MGT 233 Digitalanzeiger. Two transducers were used to measure the horizontal displacement, see figure 2.1.

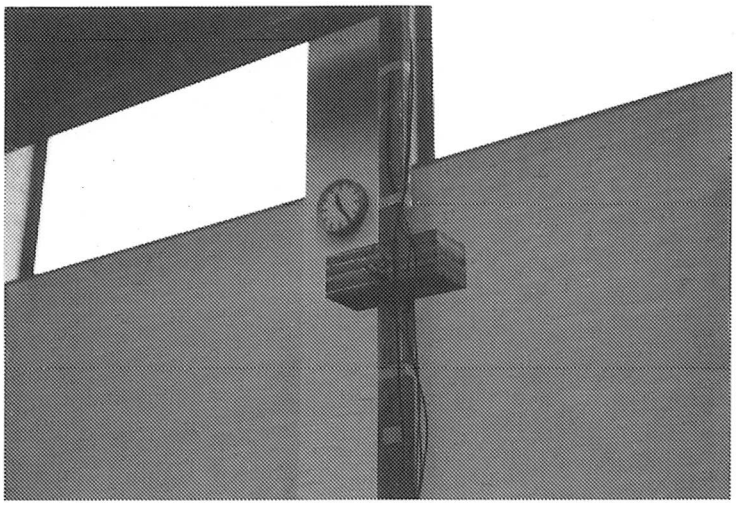

Figure 1.3. The concentrated mass, mass 1.

The response of the monopile model was measured as accelerations or displacements determined by integration of the acceleration signals. The accelerations were measured by B&K accelerometers, type 8306 (with built in amplifier) and the displacements were measured by B&K accelerometers, type 4370 with a charge amplifier, type 2625. The response was mainly measured at the two concentrated masses.

As a supplementary response information four strain gauges were placed at the bottom of the monopile model. An amplifier, type HBM MGT 231 was used.

The force between the hydraulic cylinder and the base was measured by a force transducer, type B&K 141069.

The excitation and response signals were recorded on a Teac Tape Recorder, type R80. The signals were as a quick control written out on a HP plotter, type 7402A.

As a control and analyse tool a spectrum analyser, type HP3582A was used. In the analyse of the data some of the signals were sampled, using a data acquisition board, DT2828 and analysed using a personal computer,type IBM-AT.

2 TESTING AND THE GENERAL RESULTS

In this chapter the testing and the general results will be outlined. Later in the subsequent chapters the results will be presented and discussed in details.

The experiment began with a general calibration and control of the instrumentation and excitation set-up. Afterwards the monopile was tested under different excitation forms.

The standard instrumentation consisted of an accelerometer placed on each mass and two displacement transducers. The latter were applied to measure the base displacement, see figure 2.1.

As a control the accelerometers, the accelerometers were placed at the base where the displacement transducers were placed. The acceleration as well as the displacement signals from the accelerometers corresponded very well with the displacement signal obtained from the transducers. This control was done for a sinusoidal signal with frequencies from 0.5 to 10 Hz. Only the B&K type 8306 accelerometer was able to measure frequencies from 0.5 to 0.9 Hz. It was however noticed that displacement signal determined by integration of the acceleration signal was seriously biased with respect to the phase.

As an investigation of the excitation setup it was tried to measure the vertical and sidewards base movements. This was tried with accelerometers but it turned out to be impossible because of the transversal sensitivity of these. Instead an arrangement with the three displacements transducers was used. The investigation showed no sidewards base movement, but some vertical movement especially at resonance frequencies. This indicated a significant interaction between the monopile and the base. This will be commented later in chapter 3.

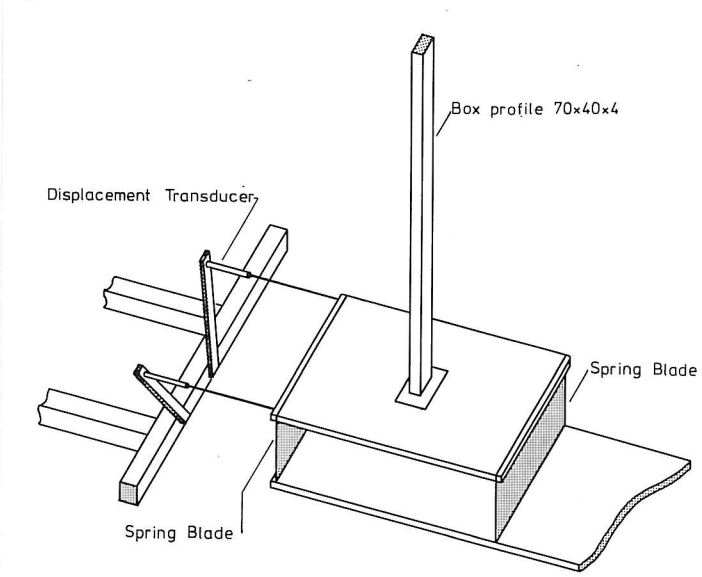

Figure 2.1. Displacement transducers at the base.

2.1 Free Vibration

A free vibration of the monopile was created by a push with the hands. The free vibration is shown in figure 2.2 for the displacement of mass 1. The figure shows that the monopile is lightly damped with a first eigen frequency about 1.10 Hz in the first main direction. The first eigen frequency in the second main direction was also found by free vibration to about 1.65 Hz.

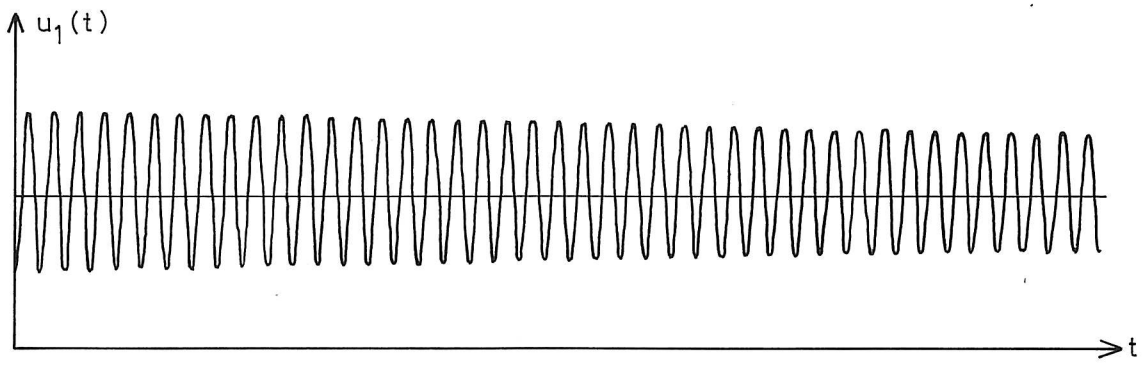

Figure 2.2. Free vibration for the displacement of mass 1 in the first main direction.

2.2 Sinusoidal excitation

The magnitudes of the first two eigen frequencies in the first main direction were further investigated by a sinusoidal excitation of the base. The input frequency was varied from 0.5 to 10 Hz. The first and second eigen frequency were determined to be about 1.10 and 7.20 Hz respectively.

Transfer functions between the displacement of the masses and the base displacement were determined from the recorded signals. The result for mass 1 is shown in figure 2.3. The results were not quite reliable because of two reasons. Firstly, it was found that it was difficult to tune the input frequency precisely because of some sort of interaction between the monopile and the excitation system. Secondly, the response was not quite stationary due to the low damping of the monopile. This was especially a problem after having passed a resonance frequency. It was necessary to wait a long time before stationary signals were obtained approximately after having changed the input frequency. In fact the experience was, that the use of sine sweep was in general not suitable for this construction.

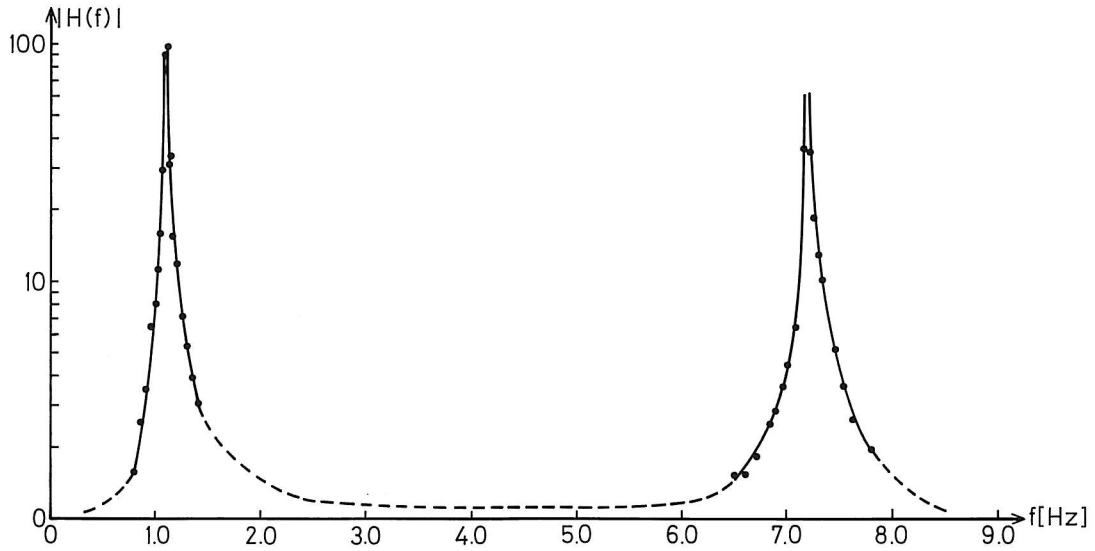

Figure 2.3. Transfer function of the displacement of mass 1. Determined from a sinusoidal excitation.

The phase between the displacement of the masses and the base displacement was also measured for a sinusoidal excitation. This was partly done by a phasemeter partly by a spectrum analyser. The phase function of the displacement of mass 1 is shown in figure 2.4. It was very difficult and uncertain to measure the phase difference at resonances because the phase was not constant. This can probably be explained by the reasons mentioned above.

The two first mode shapes in the first main direction were also measured by a sinusoidal excitation as input. This was done with four accelerometers placed along the monopile. The results are shown in figure 2.5. A further discussion of the mode shapes is given in chapter 7.

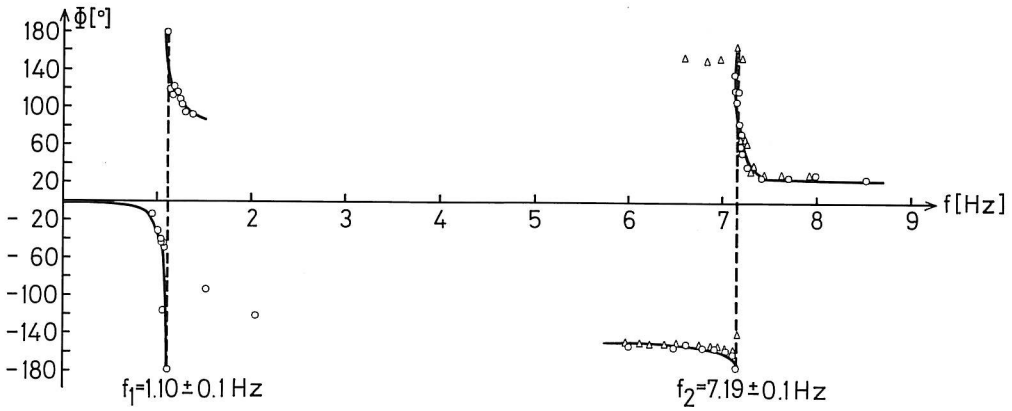

Figure 2.4. Measured phase difference between displacement of mass 1 and the base displacement for a sinusoidal excitation.

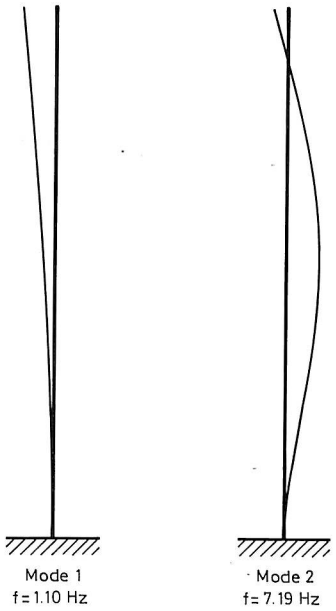

Figure 2.5. Measured mode shapes in the first main direction with a sinusoidal excitation as input.

2.3 Random excitation and FFT analysis

Random signals were also applied as base displacement and followed by a FFT analyse using the spectrum analyser. The spectrum analyser was able to compute the discrete amplitude spectre, the transfer function, the phase function and the coherency function.

White noise and periodic noise signals from the spectrum analyser were applied as input signals. These signals were filtered before they were applied as input to the control system of the hydraulic system. The cutoff frequency was typical 3 or 15 Hz. depending on the wanted response of the monopile. The noise source signal after having passed the lowpass filter but before the hydraulic system is shown in figure 2.6.

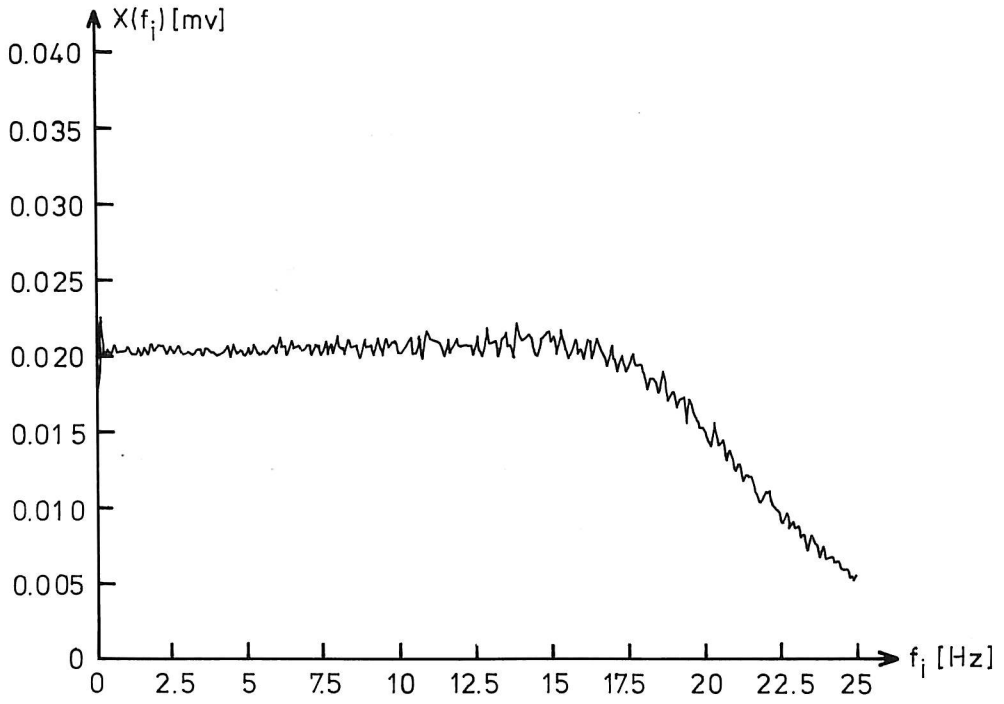

Figure 2.6. Frequency analysis of periodic noise having passed a 12 Hz lowpass filter.

The difference between white and periodic noise is that the periodic noise is created as a random signal with a period corresponding to the sampling time of the time series given by the chosen frequency area of the spectrum analyser. The finite length of the time series means a finite resolution of the input spectrum due to the relation $\Delta f = \frac{1}{T}$. The white noise signal is different because it has a substantial longer period and therefore an input spectrum with an almost infinite resolution. This difference means two things. Firstly, the smaller period of the periodic noise means that averaging is not so urgent as for real white noise. Secondly, the finite resolution of the input spectrum of the periodic noise means that there is a risk that narrow banded responses will not be properly stimulated. Both noise sources have been applied in the experiment because of their advantages and disadvantages.

The use of frequency analysis in the experiment made it important to be aware

on the following points :

1. Stationary input and output.
2. Choice of window functions in the FFT analysis.
3. Sufficient frequency resolution.
4. Sufficient averaging of the FFT data.

Point one was easily obtained because the input source and the system were stationary when the input was white or periodic noise.

The proper choice of a window function depended on the input signal. If the white noise source was applied, a Hanning window was chosen. If the periodic noise was applied a uniform window was used.

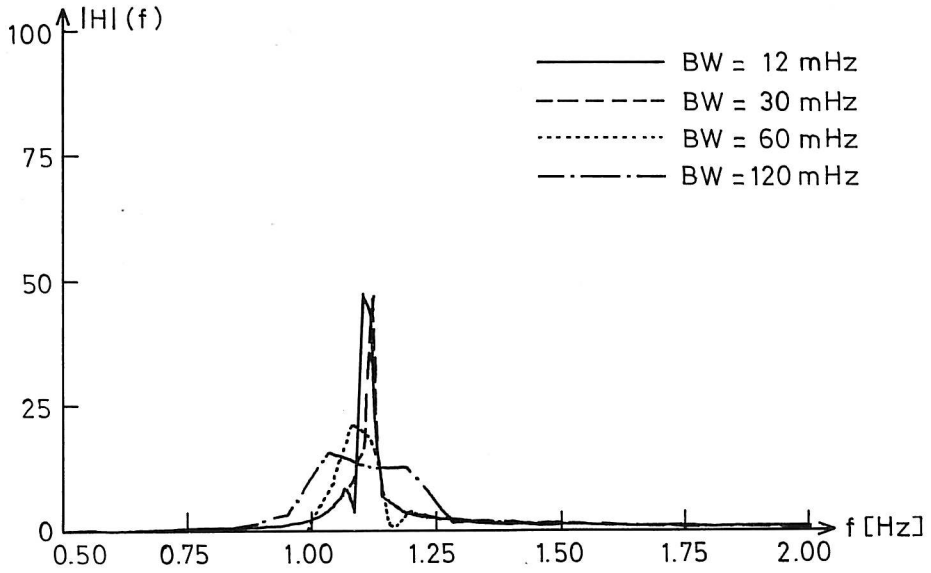

Figure 2.7 Transfer function between acceleration of mass 1 and the base displacement for different choice of frequency resolution. Excitation source: White noise.

The critical point in the use of frequency analysis was the frequency resolution. This was the case because the monopile was very lightly damped. The importance of frequency resolution is illustrated in figure 2.7, where the transfer function between acceleration of mass 1 and the base displacement is shown. The figure shows the influence of different frequency resolution given by an effective bandwidth. It is seen that at least a resolution of 30 mHz. was a necessary. This level of resolution was only obtainable for frequencies under 2.5 Hz. An effective bandwidth of 60 mHz was applied for frequencies above 2.5 Hz. When the uniform window was applied corresponding to periodic noise the resolution was a somewhat better but

not sufficient. As a consequence the results must be used with care.

The averaging of the transfer functions was done as RMS averaging for the transfer function and as ordinary linear averaging for the phase function. The number of averages and resolution etc. applied in the frequency analysis are shown in table 2.1.

Input base displ.	Response type	BW_{eff} Hz	Number of averages	Filter cutoff frequency hz
Periodic noise	M_1 acc.	0.02/0.04	4/32	3/12
-	M_2 acc.	0.02/0.04	8/32	3/12
-	M_1 displ.	0.04	8	15
-	M_2 displ.	0.04	8	15
White noise	M_1 acc.	0.06	16	15
-	M_1 displ.	0.03/0.06	8	15

Table 2.1. The performed frequency analysis. See also enclosure 1.

Figure 2.8 shows an example of the determined transfer and phase functions for the acceleration response of mass 2 with the base displacement as input. The functions look very nice corresponding to a system of two degrees of freedom. It should be noticed that the base displacement has been included in the measured transfer and phase function, because the measured response also contained the base movement.

The coherence function is also shown in figure 2.8. It expresses the correlation between input and output. The figure shows that the coherence is low and fluctuating from 0.0 to 0.5 Hz and from 4.48 Hz. In the region up to 0.5 Hz this is due to the failure of the accelerometers in the low frequency region. At 1.5 Hz the coherence drops suddenly. This is because an antiresonance is found at this frequency. That means the response is low which means that signal noise leads to the low coherence. From 4.48 Hz the fluctuating coherence is caused by insufficient resolution. So the coherence function clearly indicates when something is wrong in the analysis. The lack of resolution is also recognised in the figures of the transfer and phase functions which show a fluctuating picture from 4.48 Hz and upwards.

The FFT results presented in figure 2.8 are rather typical results of the analysis of the measurements. Therefore, it is necessary to take the FFT results with some caution in the analysis of the measurements. Consequently the performed FFT analysis is an important subject in the following chapters.

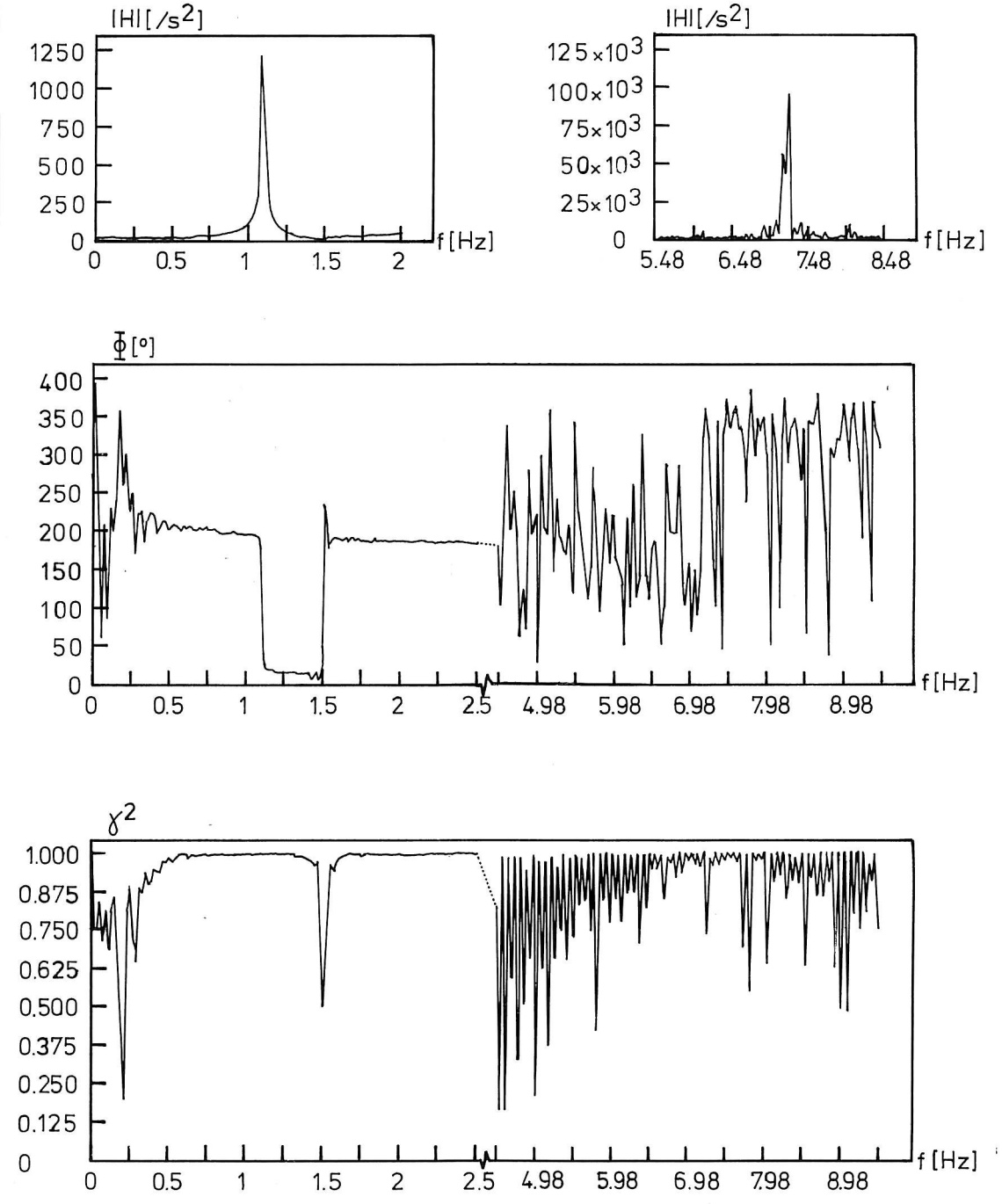

Figure 2.8. The results of the FFT analysis of the acceleration response of mass 2 with periodic noise excitation.

2.4 Fatigue of the monopile

During the last half of the experiment a sudden decrease in the eigen frequencies was noticed. At the end of the experiment the reason was detected. A fatigue crack had developed above the weld at the foot of the monopile, see figure 2.9. The crack had grown more than half the way through the box profile of the monopile. This explains the sudden decrease in the eigen frequencies. The importance of this accident was investigated by a free vibration test. From this test eigen frequencies and damping ratios were estimated, see chapter 5.5, 6.6 and 7.0 . The fatigue occurrence means that the structure of the monopile was not stationary. The interpretation of the results has therefore become a little more difficult and uncertain than expected.

After having finished the experiment there is no doubt that the fatigue crack mainly was caused by the sinusoidal excitations of the monopile. The excitation level has been to high and could have been chosen to be considerable smaller. However this is an experience which should be used in the future.

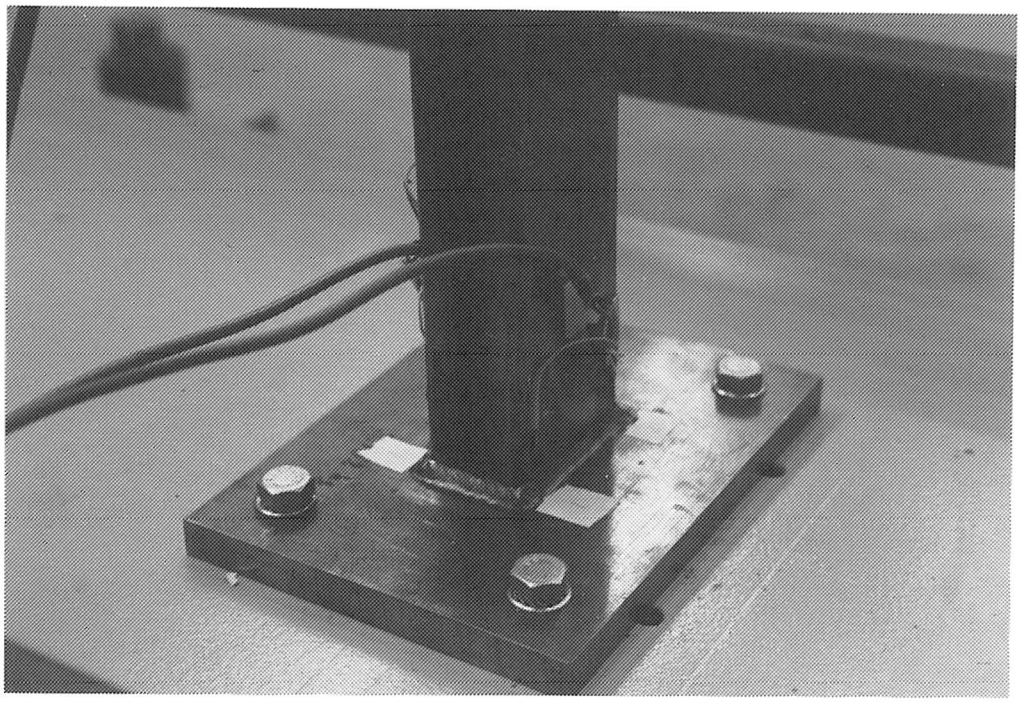

Figure 2.9. The bottom of the monopile where fatigue occurred.

3 INTERACTION BETWEEN BASE AND MODEL

Some sort of interaction between the monopile model and the base was detected early in the dynamic testing of the model. It was noticed that it was difficult to choose an exact frequency as input frequency. Furthermore, it was found that the second eigen mode had a very strong influence on the input signal. This is shown in the discrete amplitude spectrum of the base displacement, see figure 3.1.

3.1 The state of equilibrium

As an investigation of this phenomena a force transducer, type B&K 141069 was placed between the cylinder and the base. The purpose was to determine the interaction between the monopile model and the base displacement. In this test the base displacement, the cylinder force, and the acceleration of the two masses were recorded. The test was performed with an input frequency corresponding to first and second eigen frequency respectively. The signals were recorded on a tape recorder.

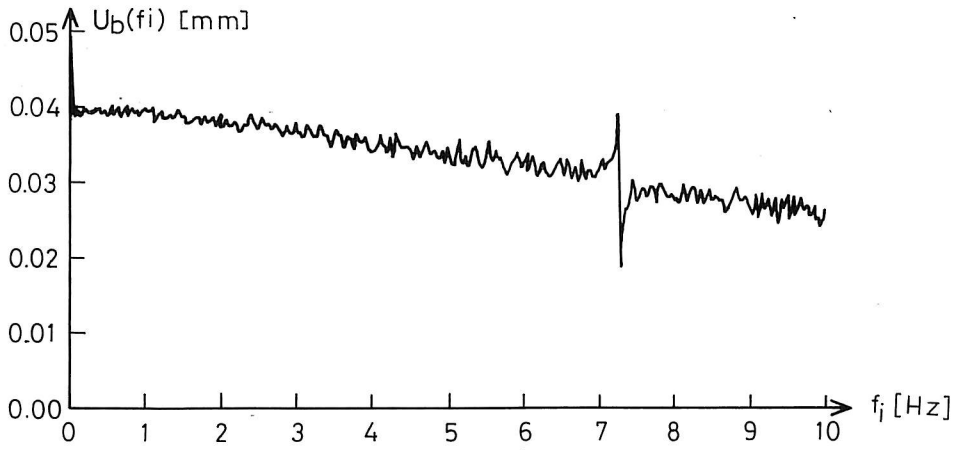

Figure 3.1. Discrete Amplitude Spectrum for the Base Displacement.

In figure 3.2 and 3.3 the recorded signals are shown for an input frequency corresponding to 1.10 Hz and 6.98 Hz respectively. It was noticed that the force signal of the cylinder was not immediately stationary. The cylinder system clearly needed some time to adapt to the dynamic response of the monopile model before a stationary situation had been created. Secondly the force signal was not a pure sinusoidal signal. The displacement signal looked more like a sinusoidal signal even though some disturbance could be recognized. The distortion of the sinusoidal signal is probably due to the adaptation process between the cylinder and the model.

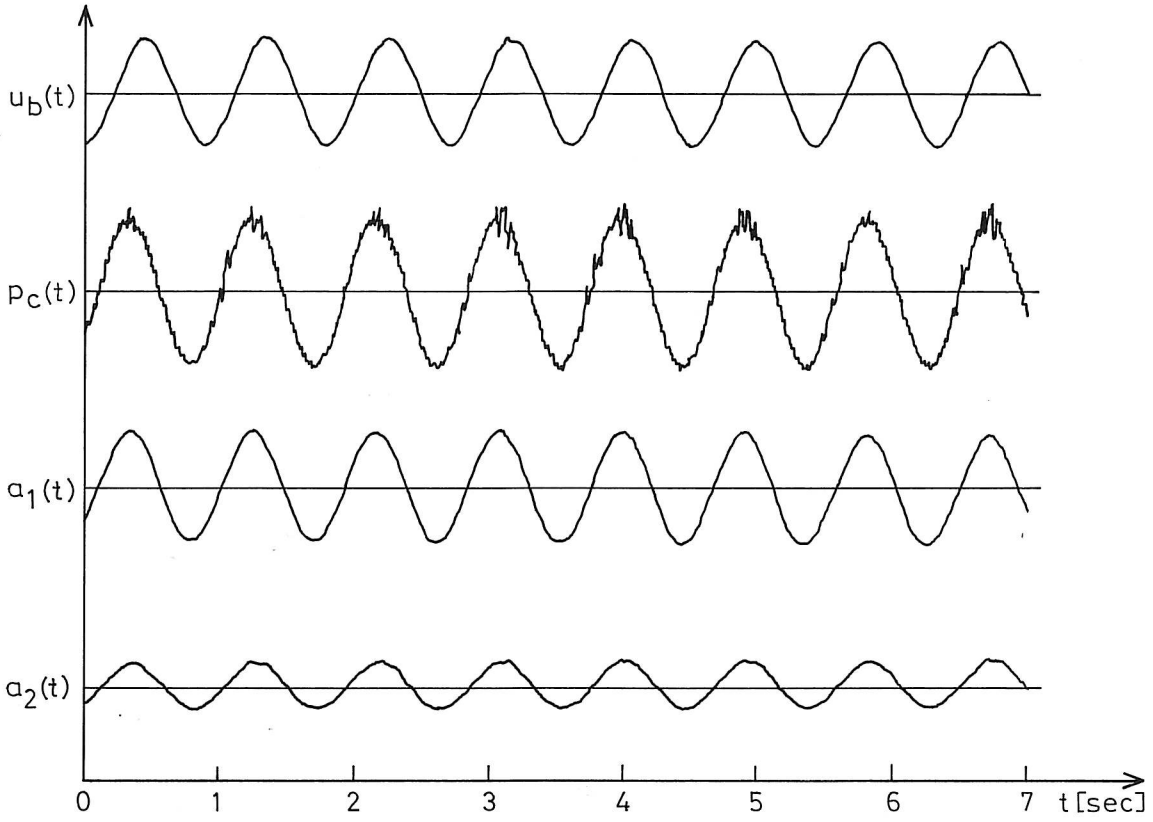

Figure 3.2. Recorded Signals at 1.10 Hz.

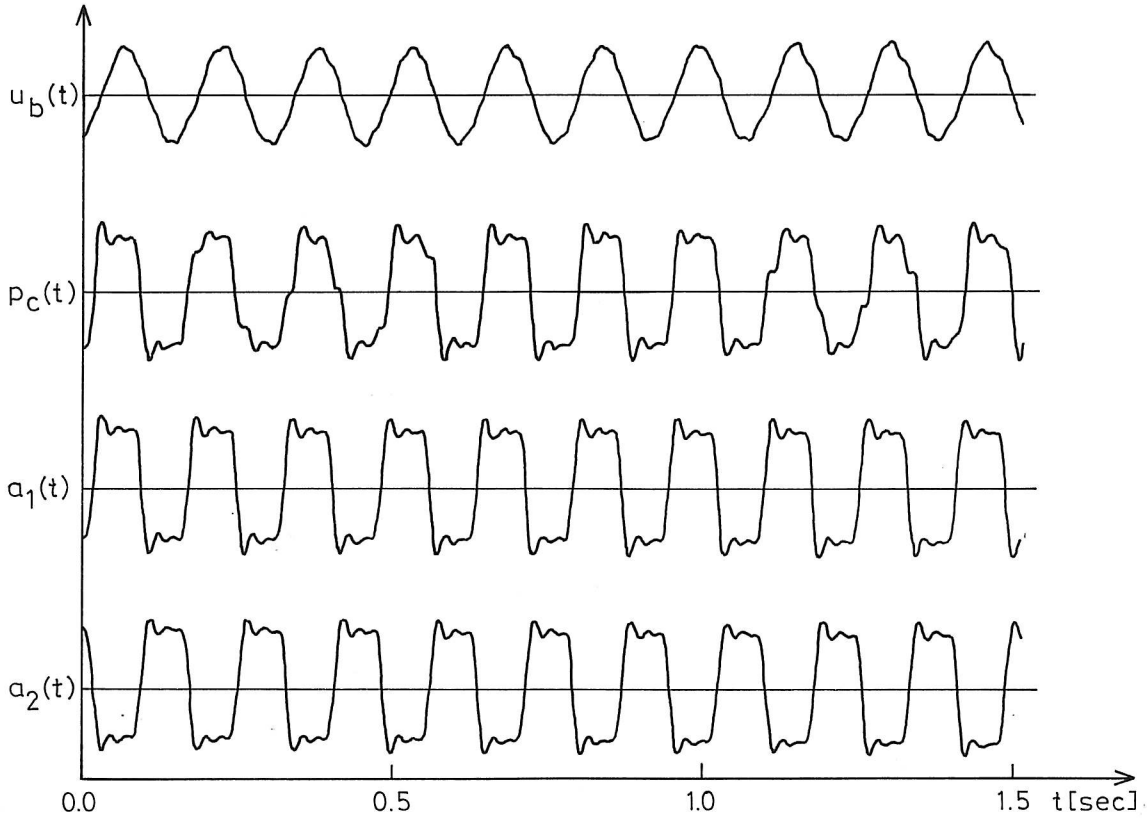

Figure 3.3. Recorded Signals at 6.98 Hz.

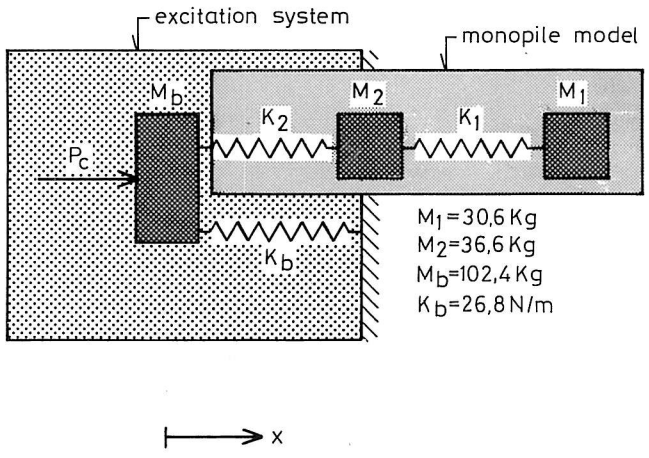

Figure 3.4. Model of the dynamic system.

As a further investigation of the interaction problem a dynamic model of the hole

system was considered, see figure 3.4. The model included the monopile model, the mass of the base, the base springs and the cylinder force. The model was assumed to be linear and no damping forces were assumed to be present. From the three equations of motion the following relation has been obtained:

$$M_b\ddot{x}_b = P_c - k_b x_b - M_2\ddot{x}_2 - M_1\ddot{x}_1 \tag{3.1}$$

The phase differences between the four signals at the two resonances are shown in table 3.1. They have been corrected for the phase distortion caused by the measuring procedure. The phase difference between the two mass accelerations corresponds to the two eigen modes.

From the time signals shown in figure 3.2 and 3.3 it is clearly seen, that the signals hardly can been approximated by sinusoidal signals with given amplitudes. However, it has been chosen to use the RMS-values of the spectre to estimate an amplitude for a sinusoidal signal. The estimated amplitude is found as $A = \sqrt{2E[x^2]}$.

Frequency Hz	Φ_{x_b} °	Φ_{P_c} °	$\Phi_{\ddot{x}_1}$ °	$\Phi_{\ddot{x}_2}$ °
1.10	0	29	11	11
6.98	0	45-52	-152	24

Table 3.1. Phase differences between signals. Correction for phase distortion has been made.

Frequency Hz	$E[x_b^2]$ mm^2	$E[P_c^2]$ N^2	$E[\ddot{x}_1^2]$ $(m/s_2)^2$	$E[\ddot{x}_2^2]$ $(m/s^2)^2$
1.10	0.4677 (4.70)	3238.6 (70.4)	1.6928 (55.2)	0.2838 (27.0)
6.98	0.4140 (179.2)	22874.1 (144.5)	30.6897 (211.4)	29.7454 (257.81)

Table 3.2. Mean square values. The numbers in ( ) are the corresponding force amplitude (N). The force amplitude from the base spring was computed to 26.0 N and 25.9 N for the frequencies 1.10 Hz and 6.98 Hz, respectively.

As a measure of the deviation from equilibrium of the forces in (3.1) a ratio has been applied. The denominator was chosen as the positive part of (3.1) when all the terms were placed on the left side of the equality sign and the numerator was the sum of the terms corresponding to the deviation from zero. From table 3.2 the deviation from equilibrium of the forces has been found to be:

1.10 Hz:

$$\frac{M_b\ddot{x}_b + M_1\ddot{x}_1 + M_2\ddot{x}_2 + k_b x_b - P_c}{M_b\ddot{x}_b + M_1\ddot{x}_1 + M_2\ddot{x}_2} = -9.5\%$$

6.98 Hz:

$$\frac{M_b\ddot{x}_b + M_1\ddot{x}_1 - M_2\ddot{x}_2 + k_b x_b - P_c}{M_b\ddot{x}_b + M_1\ddot{x}_1} = -6.6\%$$

The equilibrium equations are seen to be satisfied approximately. The deviations might be due to the approximation of the signals to sinusoidal signals or damping forces which have not been included in the model.

3.2 The vertical and rotational displacements

The interaction between the monopile model and the base was also considered in relation to the vertical movement of the base. The vertical displacements were measured by displacement transducers. It was impossible to use accelerometers because of the transversal sensitivity of the applied type of accelerometers. The vertical displacements were measured at three points of the base plate for the two eigen frequencies 1.10 Hz and 7.20 Hz. The displacement signals were analysed in the frequency domain. The amplitude spectrum for the displacement at a base point is shown in figure 3.5 for three different input frequencies around the two eigen frequencies. It is seen from figure 3.5 that the vertical displacement reach a maximum when the input frequency corresponds to an eigen frequency. A spectral peak at 5.04 Hz is found. The source to this peak is unknown. It might be due to the way the displacement transducers were fixed to the ground.

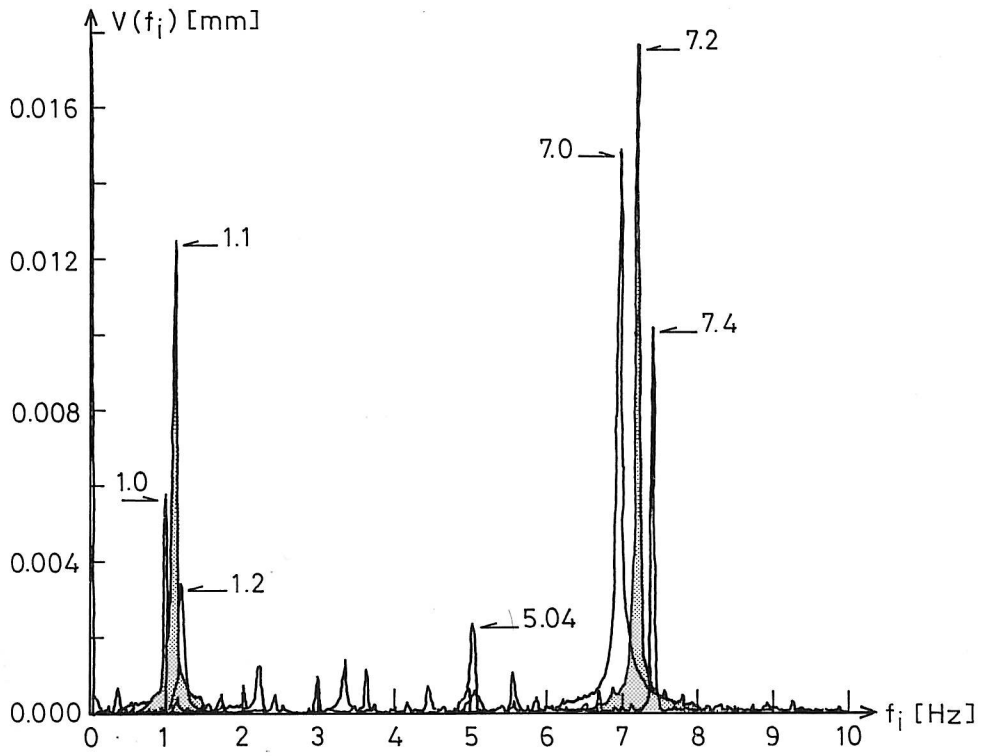

Figure 3.5 Discrete amplitude spectrum for the vertical displacement of the base for different input frequencies.

Another thing to notice is the occurrence of spectral peaks at a multiple of the input frequencies. This it is seen in figure 3.5 but is perhaps more pronounced in figure 3.6, where the amplitude spectrum of the vertical mean displacement is shown. The same characteristic peaks are found in almost any signal. If one analyses the signal from a sine generator one finds also the same peaks. Because it was possible to remove these peaks by a filter the conclusion is that the characteristic peaks arise in the signal generator and not the spectrum analyser. That is, the regulation system of the cylinder is the source to these peaks at a multiple of the input frequency. However it can be concluded that these subharmonics are without any importance in comparison with the energy at the input frequencies.

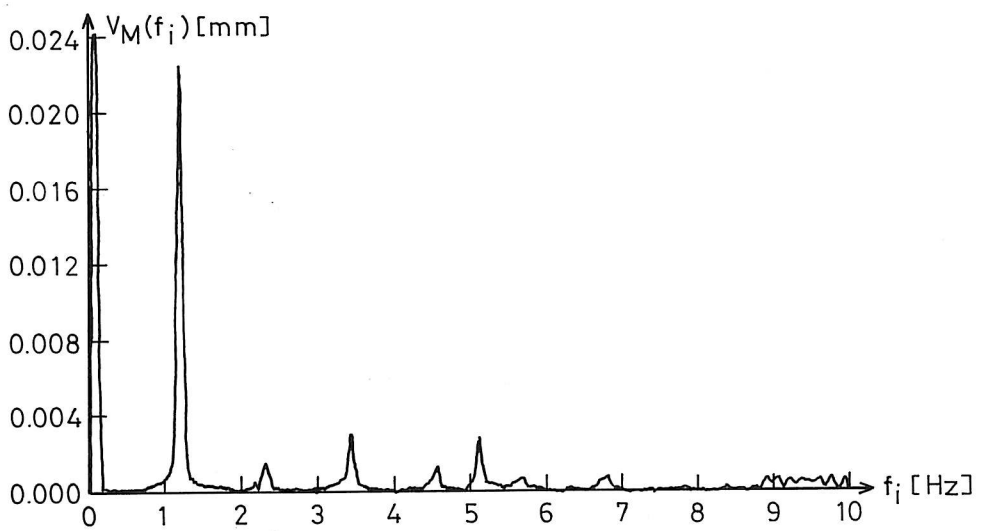

Figure 3.6 Discrete amplitude spectrum for the vertical mean displacement of the base at 1.10 Hz as input frequency.

The magnitude of the vertical displacement of the base has been estimated. This has been done by approximating the amplitude spectrum, shown in figure 3.6 by a sinusoidal signal. This procedure was shown in the previous section. The results are shown in table 3.3. The estimated amplitude for the vertical mean displacement signal is seen to be significant, especially for the second eigen mode where the ratio between the vertical and the horizontal displacement amplitude is 12%. The ratio under a static, horizontal displacement was found to be about 1%. It follows that the second eigen mode gives a significant dynamic amplification in agreement with the previously found results.

Frequency Hz	$E[v_b^2]$ mm^2	$\Delta\hat{v}_b$ mm	$\Delta\hat{x}_b$ mm	$\Delta\hat{v}_b/\Delta\hat{x}_b$ %
1.11	0.0062	0.03	0.97	3.0
7.20	0.0006	0.11	0.91	12.1

Table 3.3. Estimated amplitude for the vertical mean displacement.

The rotation of the base has also been investigated. The rotations about the two main axes were measured as a displacement difference. The first and the second

main axis were defined as the axis parallel with the primary base movement and the orthogonal axis in the plane of the base respectively. The signals were also in this case approximated by sinusoidal signals, see table 3.4. From the table it is seen that the rotations are without any importance for the second main axis. The rotations about the first main axis were even less.

Frequency Hz	$E[dv^2]$ mm^2	A_{dv} mm	$\Delta\Theta$ °
1.11	0.003	0.08	0.0064
7.20	0.01	0.14	0.012

Table 3.4. The estimated amplitude for the rotations of the second main axis.

3.3 Conclusion

It can be concluded that some kind of interaction exists between the monopile and the hydraulic control system. This is not surprisingly because there has of course to be a state of equilibrium. So the control system has to adapt to the response of the monopile.

The interaction process explains why it is difficult to tune the input frequency around resonance. The response of the monopile is so strong that it simply controls the displacement of the base. That is another reason not to use a sine sweep excitation but a random excitation. The interaction effect causes also an increased vertical displacement at resonance. This however, seemed not to be of great importance. The point to be kept in mind is that the interaction means that an adaptation process has to take place and this takes time. Consequently one has to be aware of whether the signals have become stationary or not. If not this may cause confusing and misleading results.

4 MODELLING AND IDENTIFICATION

In this chapter the applied models and system identification methods will be introduced. A detailed explanation and discussion will not be given. Further explanation and discussion can be found in the given references.

A theoretical model is needed when an experiment is planned and performed. It is necessary because some a priori knowledge is needed to make sensible tests and interpretations of the test results. The latter may also be called system identification.

This chapter will first give a brief explanation of the theoretical model and then introduce the applied system identification methods. Finally two computational models of the monopile model will be given.

4.1 General model

The general assumption has been that the monopile response can be described by the system of equations:

$$\overline{\overline{M}}\ddot{\overline{x}} + \overline{\overline{C}}\dot{\overline{x}} + \overline{\overline{K}}\overline{x} = \overline{f} \tag{4.1}$$

Only translation degrees of freedom have been considered in the model and only the bending stiffness has been taken into account.

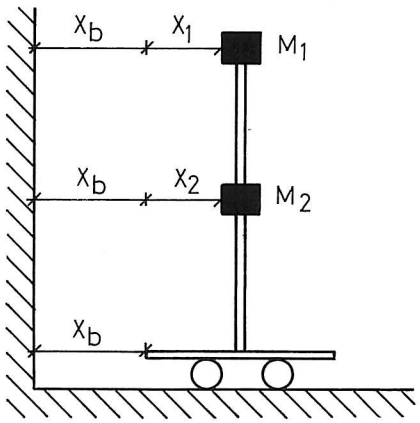

Figure 4.1. Base excitation of the system

In the experiment the excitation was mainly created by displacement of the base, see figure 4.1. The measured response of the monopile was given by :

$$\overline{y} = \overline{x} + x_b\overline{g} \tag{4.2}$$

where x_b is the base displacement and $\overline{g}$ is a vector with elements of 1 for the degrees of freedom parallel to the excitation direction. Otherwise the elements are zero. In the present case no zero elements were applied.

The form of the excitation, $\overline{f}$ due to the base displacement can be found from the Lagrange's equation:

$$\Delta(T+U) = D \tag{4.3}$$

where T, the kinetic energy, U, the potential energy and D, the work of the damping forces are given by:

$$T = \frac{\dot{\overline{y}}^T \overline{\overline{M}} \dot{\overline{y}}}{2}$$

$$U = \frac{\overline{x}^T \overline{\overline{K}} \overline{x}}{2}$$

$$D = -\overline{\overline{C}} \dot{\overline{x}} d\dot{\overline{x}}$$

which gives after some manipulations:

$$\overline{f} = -\overline{\overline{M}} \ddot{x}_b \overline{g} \tag{4.4}$$

In the model given by (4.1) the damping forces are assumed to be velocity dependent only. This has been generally accepted as a useful model although it might deviate from reality in most cases. However the point is that it is a useful model and this makes it an acceptable but not a perfect model. This is also why proportional damping has been accepted as an assumption given as:

$$\overline{\overline{C}} = \alpha \overline{\overline{M}} + \beta \overline{\overline{K}} \tag{4.5}$$

This assumption means that (4.1) can be transformed to :

$$\ddot{z}_i + 2\omega_i \zeta_i \dot{z}_i + \omega^2 z_i = \phi_{ij} f_j \tag{4.6}$$

where:

$$\overline{\overline{M}}\ddot{\overline{x}} + \overline{\overline{K}}\overline{x} = \overline{0} \tag{4.7}$$

$$\overline{x} = \overline{\overline{\Phi}}\overline{z} \tag{4.8}$$

$$\overline{\overline{\Phi}}^T \overline{\overline{M}}\,\overline{\overline{\Phi}} = \overline{\overline{I}} \tag{4.9}$$

$$\overline{\overline{\Phi}}^T \overline{\overline{K}}\,\overline{\overline{\Phi}} = (\,\omega_i^2\,) \tag{4.10}$$

$$\overline{\overline{\Phi}}^T \overline{\overline{C}}\,\overline{\overline{\Phi}} = (\,2\omega_i\zeta_i\,) \tag{4.11}$$

Here the notation on the right side of (4.10) and (4.11) means a diagonal matrix. Beside the use of base excitation free vibration has also been considered. Using the proportional damping assumption one obtains:

$$z_i = e^{-\zeta_i\omega_i t}(Ae^{i\omega_i\sqrt{1-\zeta_i^2}t} + Be^{-i\omega_i\sqrt{1-\zeta_i^2}t}) \tag{4.12}$$

where A and B are determined by the initial conditions:

$$\overline{z}(0) = \overline{\overline{\Phi}}^{-1}\overline{x}(0)$$

$$\dot{\overline{z}}(0) = \overline{\overline{\Phi}}^{-1}\dot{\overline{x}}(0)$$

4.2 Two degrees of freedom model

The monopile has been considered as a two degrees of freedom system. This has been possible because the eigen modes were clearly separated in the frequency area from 0 to 10 hz. That meant that mainly the two bending modes in the excitation direction were expected to be excited, all though two other bending modes existed in the orthogonal direction. Therefore, the base excited system was described by :

$$\begin{pmatrix} M_1 & 0 \\ 0 & M_2 \end{pmatrix}\begin{pmatrix} \ddot{x}_1 \\ \ddot{x}_2 \end{pmatrix}+\begin{pmatrix} c_1 & c_2 \\ c_3 & c_4 \end{pmatrix}\begin{pmatrix} \dot{x}_1 \\ \dot{x}_2 \end{pmatrix}+\begin{pmatrix} k_1 & k_2 \\ k_3 & k_4 \end{pmatrix}\begin{pmatrix} x_1 \\ x_2 \end{pmatrix}=\begin{pmatrix} -M_1\ddot{x}_b \\ -M_2\ddot{x}_b \end{pmatrix} \quad (4.13)$$

For the base excited two degrees of freedom system it is possible to obtain from (4.4), (4.6) and (4.8) two transfer functions between the base displacement and the response of the two masses. If a harmonic excitation is assumed frequency considerations leads to:

$$\frac{X_1}{\ddot{X}_b} = -\frac{K_{11}}{{\omega_1}^2 - \omega^2 + 2\omega_1\omega\zeta_1 i} - \frac{K_{12}}{\omega_2^2 - \omega^2 + 2\omega_2\omega\zeta_2 i} \quad (4.14a)$$

$$\frac{X_2}{\ddot{X}_b} = -\frac{K_{21}}{{\omega_1}^2 - \omega^2 + 2\omega_1\omega\zeta_1 i} - \frac{K_{22}}{\omega_2^2 - \omega^2 + 2\omega_2\omega\zeta_2 i} \quad (4.14b)$$

where X_i has been derived from the relation:

$$x_i = X_i \exp(i\omega t)$$

and:

$$K_{11} = \Phi_{11}^2 M_1 + \Phi_{11}\Phi_{12}M_2$$
$$K_{12} = \Phi_{21}^2 M_1 + \Phi_{22}\Phi_{21}M_2$$
$$K_{21} = \Phi_{12}\Phi_{11}M_1 + \Phi_{12}^2 M_2$$
$$K_{22} = \Phi_{21}\Phi_{22}M_1 + \Phi_{22}^2 M_2$$

It is seen from (4.14) that if $\omega_1 << \omega_2$ and if the damping ratios are small, it will be a good approximation to describe the transfer function in the neighbourhood around the resonance frequencies only by one of the terms in (4.14a) and (4.14b).

From (4.14) follows the useful relations:

$$\frac{X_i}{X_b} = -\frac{X_i}{\ddot{X}_b}\omega^2 \tag{4.15}$$

$$\frac{\ddot{X}_i}{X_b} = \frac{X_i}{\ddot{X}_b}\omega^4 \tag{4.16}$$

$$\frac{\dot{X}_i}{\ddot{X}_b} = \frac{X_i}{\ddot{X}_b}\omega i \tag{4.17}$$

In the experiment the displacements or the accelerations were measured corresponding to (4.15) and (4.16) respectively. Equation (4.17) was applied in the identification algorithm called circle fitting. In all cases the base movement was included in the measured signals.

4.3 System identification

Five different system identification methods have been applied to estimate the parameters in the theoretical model. All the methods use the single degree of freedom assumption. That is a lightly damped system with well separated eigen frequencies is assumed. For the actual model this is a good assumption.

The time domain as well as the frequency domain has been applied in the estimation of the parameters in the theoretical model. The identification methods have been based on the measured response at the two concentrated masses of the monopile model and the excitation given by the base displacement.

Some of the identification methods have been based on the measured response only. This has been possible in the case where the excitation was a white noise signal or in the case where the model performed a free vibration.

Because the experiment has been performed in a laboratory the masses of the model have been known. This information has been applied in one of the identification methods based on a lumped mass model. This may seem as cheating a little but however, the world outside the laboratory provides also information about the masses all though it might be uncertain. Therefore, an identification method based on a known lumped mass model should not be underestimated.

In general estimates of the eigen frequencies have easily been obtained due to FFT analysis whereas it has been possible only to obtain reliable damping estimates when more refined identification methods have been used. As a consequence the described methods concentrate on the estimation of the damping ratio.

4.4 Identification by the logarithmic decrement

A free vibration gives information about the eigen frequency and the damping ratio for the mode no. j if only this mode is excited. A variant of the logarithmic decrement for this mode is then given by:

$$\delta(n) = ln(\frac{A_n}{A_1}) \tag{4.18}$$

where the logarithmic decrement is a function of the cycle number given an amplitude for the oscillation number one. Using (4.12) one obtains:

$$\begin{aligned} \delta(n) &= \zeta_j(2\pi f_j)(n-1)\frac{2\pi}{(2\pi f_j)\sqrt{1-\zeta_j{}^2}} \\ &= 2\pi\zeta_j n - 2\pi\zeta_j \end{aligned} \tag{4.19}$$

This corresponds to a straight line with the slope $2\pi\zeta_j$ and the intersection $2\pi\zeta_j$ with the ordinate axis if $\zeta_j << 1.0$.

If the linear model is correct, the slope corresponding to the damping ratio can be shown to be normal distributed with the variance:

$$s^2 = \frac{\sum_{n=1}^{N}\left(ln(\frac{A_n}{A_1}) - (2\pi\zeta_j n - 2\pi\zeta_j)\right)^2}{N-2}\frac{1}{\sum_{n=1}^{N} n^2 - \left(\sum_{n=1}^{N} n\right)^2/N} \tag{4.20}$$

It can be noticed that the estimated mean value of the damping ratio and the eigen frequency are independent.

4.5 Identification from peak values

If the masses are assumed known it is possible to determine the damping ratios and the mode shapes from the dynamic amplification factors, D_{ij} given for each degree of freedom for each mass, see figure 4.2.

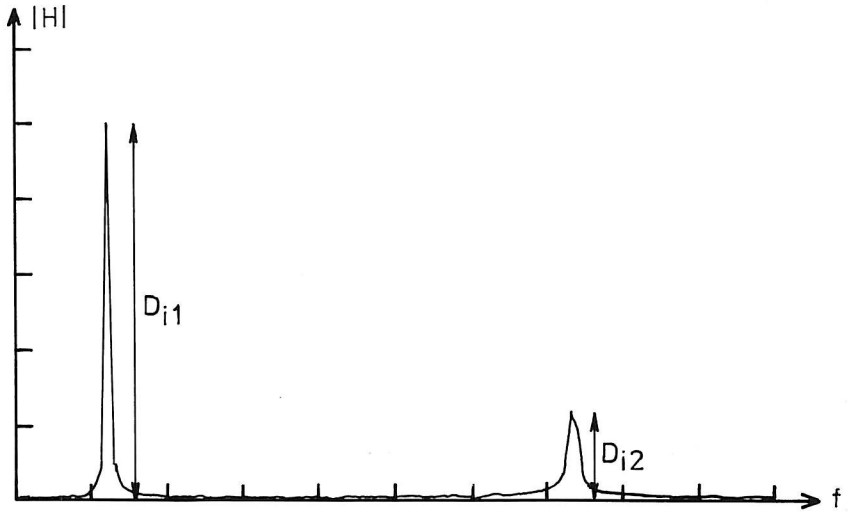

Figure 4.2. The dynamic amplification factors for the response of the i'th mass.

The method assumes that the orthogonallity conditions hold, see (4.9). At the eigen frequency number j the dynamic amplification factor is given by:

$$D_{ij} = |\frac{K_{ij}}{2\zeta_j}| \tag{4.21}$$

for mass number i. This gives the linear relation:

$$\begin{pmatrix} 2D_{11} & -2D_{12} & 0 \\ 2D_{21} & 2D_{22} & 0 \\ \frac{M_2}{M_1}2D_{12} & -2D_{12} & -(M_2 + \frac{M_2^2}{M_1}) \end{pmatrix} \begin{pmatrix} \zeta_1 \\ \zeta_2 \\ \Phi_{12}^2 \end{pmatrix} = \begin{pmatrix} 1 \\ 1 \\ 0 \end{pmatrix} \tag{4.22}$$

This system of equations gives the damping ratios and one element of the mode shape matrix. The complete mode shape matrix can be obtained from the orthogonallity conditions. The above primitive identification method assumes a lightly proportional damped system with well separated eigen frequencies. The weakness of this identification method is that it requires a great frequency resolution if the correct peak values have to be applied.

4.6 Identification from peak shapes

From (4.14) one obtains by a single degree of freedom assumption for the j'te peak:

$$|H_i(f)| = \frac{|K_{ij}|f^2}{\sqrt{(f_j^2 - f^2)^2 + 4f_j^2 f^2 \zeta_j^2}} \tag{4.23}$$

where $H_i(f)$ is the transfer function between the acceleration of the i'th mass and the base displacement. This equation can be rewritten as a straight line:

$$K_{ij}^2 - {\zeta_j}^2 x = y \tag{4.24}$$

where:

$$x = 4(\frac{f_j}{f})^2 H_i(f)^2$$

$$y = H_i(f)^2((\frac{f_j}{f})^2 - 1)^2$$

x and y refers here to the coordinates obtained from the FFT data. It is seen that the peak can be described by a straight line with the slope ${\zeta_j}^2$ and the intersection with the y-axis K_{ij}^2. However, both quantities are unknown together with the eigen frequency. But since a straight line is assumed the procedure is just to variate the eigen frequency until maximum correlation is obtained. Then the damping ratio and the constant K_{ij} can be determined.

The straight line model is only valid if the points are independent normal identical distributed around the straight line. If this is the case one can establish a confidence interval for the square of the damping ratio, which is supposed to be normal distributed. The variance of the slope is given by:

$$s^2 = \frac{\sum_{l=1}^{N}(y_l - < y_l >)^2}{N-2} \frac{1}{\sum_{l=1}^{N} x_l^2 - (\sum_{l=1}^{N} x_l)^2/N} \tag{4.25}$$

where $< y_l >$ are the predicted values and y_l and x_l are measured values.

This curve fit method of the peaks of the transfer functions is superior to a method like the half power bandwidth estimation because several points are applied.

4.7 Circle fit

In stead of identifying the model from the information hidden in the transfer function the information can be expanded to contain the phase function also. This should give a better identification. The transfer and phase function can be transformed into a real and imaginary part corresponding to the real and imaginary parts determined from (4.14) and (4.17):

$$Re[\frac{\dot{X}_i}{\ddot{X}_b}] = \frac{2K_{ij}(2\pi f_j)\zeta_j(2\pi f)^2}{((2\pi f_j)^2 - (2\pi f)^2)^2 + 4(2\pi f_j)^2\zeta_j{}^2(2\pi f)^2} \tag{4.26a}$$

$$Im[\frac{\dot{X}_i}{\ddot{X}_b}] = \frac{K_{ij}(2\pi f)((2\pi f_j)^2 - (2\pi f)^2)}{((2\pi f_j)^2 - (2\pi f)^2)^2 + 4(2\pi f_j)^2\zeta_j{}^2(2\pi f)^2} \tag{4.26b}$$

Notice the response is here given by the velocity of the masses. It can now be shown that if the imaginary part is plotted against the real part, a circle will appear, see figure 4.3. This plot is sometimes called a Nyquist plot. The single degree of freedom assumption has been applied here. The radius of the circle can be shown to be:

$$R = \frac{K_{ij}}{4(2\pi)f_j\zeta_j} \tag{4.27}$$

and the centre of the circle by:

$$\overline{C} = (\frac{K_{ij}}{4(2\pi)f_j\zeta_j}, 0) \tag{4.28}$$

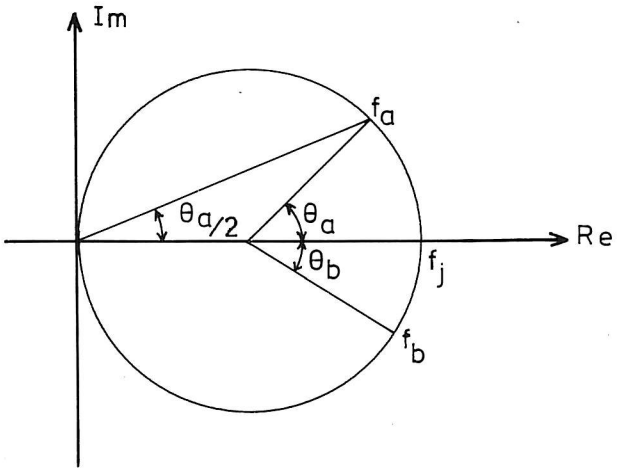

Figure 4.3. Circle fit.

If the frequency intervals of the applied FFT data are constant in the given frequency range, the damping ratio can be shown to be given by:

$$\zeta_j = \frac{((2\pi f_a)^2 - (2\pi f_b)^2)}{2(2\pi f_j)((2\pi f_a)Tan(\Theta_a/2) + (2\pi f_b)Tan(\Theta_b/2))} \tag{4.29}$$

where $\Theta_a, \Theta_b, f_a, f_b, f_j$ are given by figure 4.3. From each pair of data points a estimate of the damping ratio can be computed. If the damping ratio obtained from this method is assumed to be normal distributed, a confidence interval can be determined.

The eigen frequency, f_j can be estimated from the Nyquist plot by linear interpolation between the two points with maximum angel difference.

The shown relationship has been programmed into a computer. The circle is estimated by non-linear least square estimation. The single degree of freedom has been applied but it is possible to modify the method to several degrees of freedom. This is done as an iterative procedure where the influence of the neighbouring modes is "subtracted" from the mode of interest. This iteration process gives a quick convergence with respect to the damping ratio.

The circle fit method is described in detail in /1/.

4.8 Identification using ARMA models

In stead of performing the system identification in the frequency domain using FFT it is possible to obtain a model directly in the time domain from the sampled data. This is done by estimating an ARMA model for the response with white noise as input. Compared with the FFT analysis the advantage is that the model is obtained in the time domain given by a set of model parameters. This means for instance that an exact expression for the transfer function is obtained that is a transfer function with infinite resolution. The eigen frequency and the damping ratios can therefore be determined with great precision.

The ARMA model for a n degrees of freedom system with white noise as input is given by an ARMA model of order (2n,2n-1), that is an ARMA(2n,2n-1) model:

$$x_t - \phi_1 x_{t-1} - \phi_2 x_{t-2} \ldots \phi_{t-2n} x_{t-2n} = a_t - \theta_1 a_{t-1} - \theta_2 a_{t-2} \cdots \theta_{t-2n+1} a_{t-2n+1} \tag{4.30}$$

The Φ_i's and Θ_j's are here real constants and x_t is the sampled time series with a constant sampling rate, dt. The a_t is the discrete time series for an assumed white noise input, where a_t is independent normal identical distributed. The equivalence of this model and the system with n degrees of freedom is due to the fact that the same covariance function has been demanded for the discrete and the continuous time domain.

The ARMA model is found from sampled data using nonlinear regression. In the analyse of the sampled data a Fortran standard routine has been applied /4/.

As mentioned above it is possible to determine an autospectrum for the measured response from the estimated ARMA model. Because the input is white noise it follows that:

$$H(f) = constant\sqrt{S_{xx}} \tag{4.31}$$

where the constant depends on the excitation level. It can be shown that S_{xx} for an ARMA(2n,2n-1) model is written as:

$$S_{xx} = 2{\sigma_a}^2 dt \frac{\left|e^{(2n-1)(2\pi)fdti} - \theta_1 e^{(2n-2)(2\pi)fdti} \ldots \theta_{2n}\right|^2}{\left|e^{(2n)(2\pi)fdti} - \phi_1 e^{(2n-1)(2\pi)fdti} \ldots \phi_{2n}\right|^2} \tag{4.32}$$

where

$$0 \leq f \leq \frac{1}{2dt}$$

From this analytical expression for a n degrees of freedom system it is possible to obtain the eigen frequencies and the damping ratios exactly for the model. This can for instance be done with the peak shape method with 1.00 as correlation coefficient. It is however also possible to obtain the eigen frequencies and the damping ratios directly from the estimated ARMA parameters, which have been done in /2/.

The theoretical background for ARMA is described in /2/ and /3/.

4.9 Computational models

When planning the experiment and the system identification showed a need for a priori knowledge about the monopile. This was provided first by a simple lumped mass model with two degrees of freedom and later by a finite element model. The two models were based on information about the masses and the applied box profile. The result was information about the eigen frequencies and the mode shapes.

The lumped masses were determined as the sum of the concentrated masses and some contribution from the mass of the box profile. Mass 1 and mass 2 consisted of $\frac{1}{4}$ and $\frac{2}{4}$ of the box profiles mass respectively, see figure 3.4. The stiffness was determined from the flexibility matrix for a clamped beam. The lumped mass model with two degrees of freedom is shown in figure 4.4.

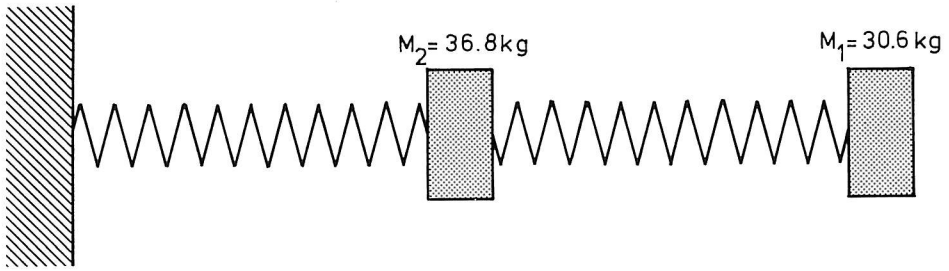

Figure 4.4. Lumped mass model.

The above lumped mass model corresponded to the monopile excited in the first main direction. As a further investigation a lumped mass model was also made for excitation in the second main direction. The results for the two lumped mass models are shown in table 4.1.

	1 Main direction		2 Main direction	
f_j hz	1.20	7.44	1.89	11.56
$\Phi_{(j)1}$	1.00	0.39	1.00	0.40
$\Phi_{(j)2}$	0.32	-1.00	0.32	-1.00

Table 4.1. Results for the lumped mass models.

The finite element model consisted of a beam model with 96 degrees of freedom connected with a plate model with 27 degrees of freedom. The plate model simulated the foot plate of the monopile. The model is shown in figure 4.5. The finite element program IMAGES /5/ was applied to determine the eigen frequencies and the mode shapes. Ten modes were computed. The results for the first four eigen frequencies are shown in table 4.2.

The results of the lumped mass models and the finite element model have been applied partly as a priori information partly in the analyse and comparison of the results obtained by system identification, see especially chapter 5,7 and 8.

	1 Main direction		2 Main direction	
f_j hz	1.15	7.11	1.64	10.43
$\Phi_{(j)1}$	1.00	0.48	1.00	-
$\Phi_{(j)2}$	0.34	-1.00	0.37	-

Table 4.2. Results for the finite element model.

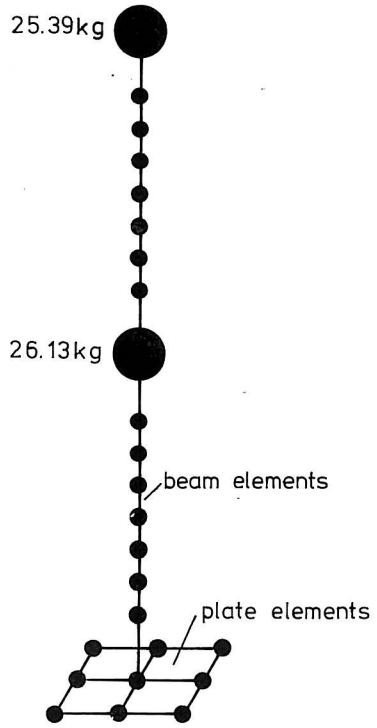

Figure 4.5. Finite element model with beam and plate elements. The weight of the small masses of the monopile is 1.58 kg and the weights of a plate element is 0.22 kg and 0.44 kg. The box profile has the dimensions 70-40-4 with a length of 4 meter.

5 IDENTIFICATION OF THE EIGEN FREQUENCIES

The eigen frequencies of the monopile were easily identified because the eigen frequencies were clearly separated. That meant also that it only was the eigen modes in the first main direction which were excited.

The monopile was assumed to be lightly damped which meant that the eigen frequencies could be determined as the frequencies which gave the maximum amplification of the response. Consequently the magnitude of the eigen frequencies was quickly estimated by a sine sweep from 0 to 10 Hz, where the amplification was noticed by eyes and ears. The two first eigen frequencies in the first main direction were found to be about 1.10 Hz and 7.19 Hz. respectively.

As an investigation of the uncertainty of the identification of eigen frequencies different types of excitation and identification methods were applied.

5.1 Free vibration

A free vibration was created by making the monopile vibrate. This was done by hand. After the free vibration had stabilized the displacement signals of the masses were written out on a plotter. From the plot the first eigen frequency was identified as 1.09 Hz.. This average value was somewhat uncertain due to the visual estimation procedure.

5.2 Sine sweep

The amplification of the monopile due to a sinusoidal input was investigated in the frequency range round the two eigen frequencies. The displacements of the masses and the base were recorded for input frequencies from about 0.9 Hz to 8.0 Hz. From theses records transfer functions were found. The phase functions were found using FFT analysis. The estimated eigen frequencies are shown in table 5.1
.

The sine sweep principal was found to be very time consuming due to the low damping of the system. After each frequency shift, stationary response was only obtained very slowly. That might have given some distortion of the found eigen frequencies.

5.3 Noise excitation

A periodic or white noise excitation was applied to the base and the displacement or the acceleration of the masses was measured. The corresponding transfer functions were then determined by FFT. The peak shape method gave the eigen frequencies as the peak frequency at which maximum correlation was obtained. The results are shown in table 5.1, page 40 for different FFT data.

5.4 ARMA models

Given a white noise excitation input an ARMA model of the displacement response of the masses was estimated.

From the estimated ARMA model it is possible to obtain the eigen frequencies and damping ratios directly from the estimated ARMA parameters. However, in the actual case it was chosen to use the estimated parameters to obtain a response spectrum and due to the white noise excitation a frequency response function, see figure 5.1.

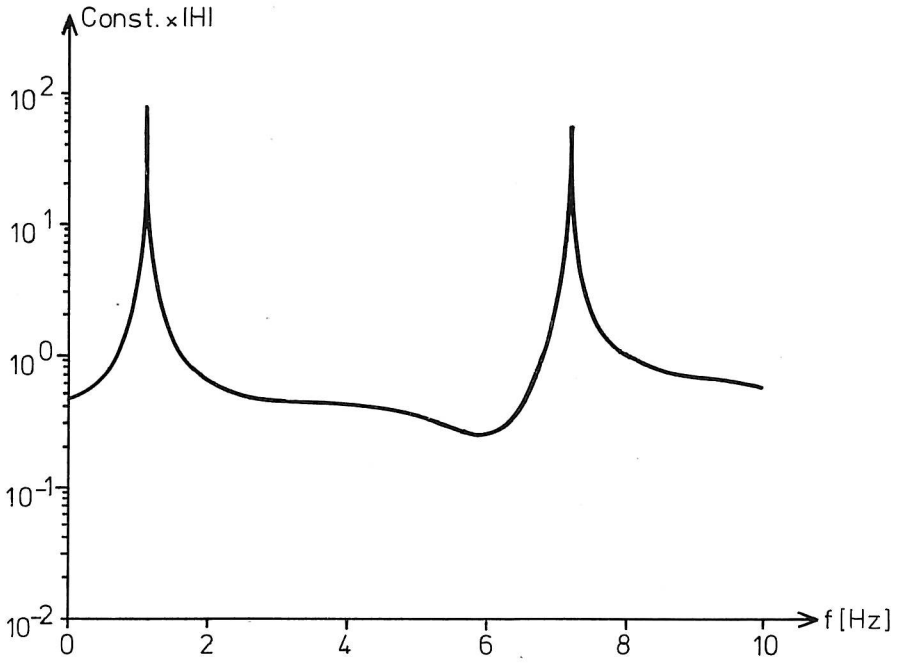

Figure 5.1. Frequency response function of mass 1. ARMA(14, 13) model estimated from white noise response. Sampling rate 40 Hz.

The order of the ARMA model was chosen so that it was consistent with n degrees of freedom system, that is an ARMA(2n,2n-1) model. Consequently even the most simple identification method should give the correct eigen frequency (and damping ratio) corresponding to the estimated ARMA parameters. In other words the estimation error in this stage should be zero.

In the actual case the base displacement signal was only approximately white noise due to several factors, see figure 3.1. Important factors have been effects such as the filtering due to the hydraulic system and the interaction between the model and the system. Furthermore, the measured mass displacement signals were

distorted. The latter was due to integration of the acceleration signals obtaining displacement signals and the failure of the accelerometers at the low frequency region (less than 0.9 Hz.).

More important however, the theory of identification using ARMA model assumes a white noise force signal. In the actual case the white noise was the base displacement signal whereas the force spectrum was something like a fourth order polynomials with minimum at 0 Hz. and increasing with frequency, see figure 5.2 a and b:

$$S_{ff} = S_0(2\pi f)^4 \tag{5.1}$$

This means that the white noise assumption will be only reasonable to assume locally around the resonance peak if the system is lightly damped. Assuming white noise with this violation means that the second eigen mode will apparently be the dominating mode in the model and perhaps lead to very uncertain information about the first mode.

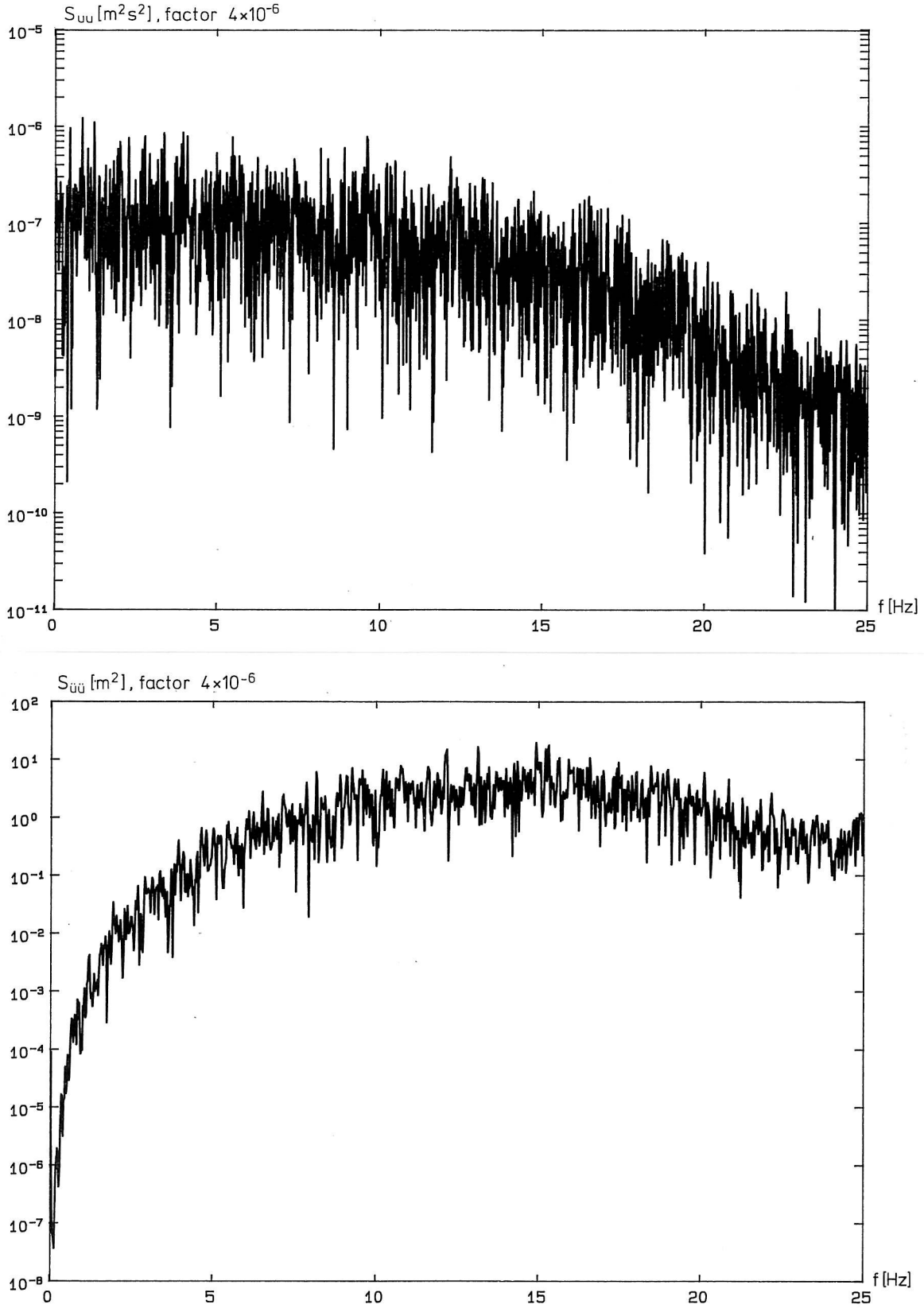

Figure 5.2. Top: Autospectrum of the base displacement. Bottom: Autospectrum of the base acceleration.

The estimation of the ARMA models was made using the NAG library, /4/. The response signals, which were applied, were sampled with 40 and 60 Hz. for mass 1 and 2 respectively. Before sampling they were filtered with a cutoff frequency about 12 Hz. .

The satisfactory model order was determined from the model error which was given by the relative residue. When the model error had obtained a minimum the model order was considered as being satisfactory.

In the actual case the sufficient model was determined to be an ARMA(14,13), see 6.5. The theoretical sufficient model was supposed to be an ARMA(4,3) corresponding to two degrees of freedom. It is thought that the high model order is due to the violated white noise. As mentioned above this can also explain why the identification of the first eigen frequency only was possible at a relative high model order.

The identified eigen frequencies from the ARMA(14,13) model are shown in table 5.1, page 40. It is seen that the estimates from the ARMA models of the two samples agree within 0.15% which is very satisfactory indeed.

5.5 Conclusion

Table 5.1 shows in general that the eigen frequencies have been determined with only small deviations. Among the identified eigen frequencies the deviation is less than 3% .

It is seen from table 5.1 that the sine sweep results all give too small eigen frequencies compared with the other results. The explanation might be that the obtained response was not stationary because the sine sweep was performed too fast.

The results based on FFT analysis show some deviation compared with each other. Insufficient frequency resolution and averaging could be an explanation. However, another explanation might be initial fatigue at the foot of the monopile model. The FFT based results are shown in chronological order and show a decreasing trend in the identified frequencies.

At the end of the experiment a fatigue crack was found at foot of the monopile above the weld. It had grown more than half the way through the box profile. A frequency analysis of a free vibration showed that the first and second eigen frequency had decreased to 0.93 and 6.56 Hz respectively. This significant reduction shows that the trend in table 5.1 could be due to fatigue. The effect of fatigue is further commented in chapter 6.

The results from the ARMA models have been obtained at the same stage as FFT analysis of the mass displacements. It is seen that the estimated eigen frequencies are a little smaller than those determined from the FFT analysis.

The identified eigen frequencies can also be compared with theoretical results found from a lumped mass model and a finite element model, see chapter 4. From table 5.1 it is seen that the lumped mass model gives too high eigen frequencies

corresponding to a maximum deviation about 9%. The finite element model gives deviations smaller than 5%. In both cases this deviation is less for the second eigen frequency. This magnitude of deviation must be said to be satisfactory.

The deviation between the identified eigen frequencies and the theoretical values must be explained by the models. The most plausible explanation is that the clamp beam assumption is an approximation to reality.

It can be concluded that the eigen frequencies have been identified successfully within $\pm 1\%$. This is quite satisfactory although it is likely that the eigen frequencies can be determined even more precisely for the given system.

The deviation between identification from measurement and theory is also acceptable bearing in mind that the applied theoretical model has not been very sophisticated. More refined models would without doubt give better results.

	f_1 (Hz)	f_2 (Hz)
Free vibration (average frequency from plot)	1.09	-
Sinus sweep (peak frequency of transfer function, mass 1)	1.09	7.17
Sinus sweep (peak frequency of transfer function, mass 2)	1.08	7.19
Sinus sweep (phase shift of phase function, mass 1)	1.10	7.19
Transfer function for displacement of mass 1 (FFT), periodic noise, (peak shape method).	1.117	7.203
Transfer function for acceleration of mass 1 (FFT), periodic noise, (peak shape method).	1.105	7.190
Transfer function for acceleration of mass 1 (FFT), white noise, (peak shape method).	1.089	7.168
ARMA(14,13), mass 1 40 Hz sampling rate	1.1054	7.1921
ARMA(14,13), mass 2 60 Hz sampling rate	1.1070	7.1900
Lumped mass model	1.20	7.44
Finite element model	1.15	7.11

Table 5.1. The identified eigen frequencies in the first main direction.

6 ESTIMATION OF THE DAMPING

While it is relative easy to explain the magnitude of eigen frequencies theoretically it is considerably more difficult to explain the damping of a construction. It is "just" all the mechanisms that lead to an energy loss of a dynamic excited structures. This means that identification is based on simple models which may be far from reality. Therefore one should not be surprised to get uncertain and somewhat confusing results.

The present structure is assumed to be lightly damped. The usual damping model is chosen, consequently the system is supposed to be proportionally damped with viscous damping. This is reasonably because the physics of the damping mechanism is not fully understood. Furthermore the damping is supposed to be small and consequently the level of modelling less important. On the other hand it is clear that the price of a simple damping model is uncertain identification of the damping. In the extreme case this may lead to absurd results such as a negative damping ratio.

6.1 Free vibration

The method of the logarithmic decrement was applied to determine the damping ratio. The monopile was excited by hand. The first eigen mode in the first main direction was excited. After the free vibration had stabilised the displacement signal of the mass 1 was written out on a plotter, see figure 2.2.

30 amplitude values corresponding to each fifth oscillation were applied to estimate the damping ratio of the first eigen mode. The relative logarithmic decrement as a function of the oscillation number is shown in figure 6.1.

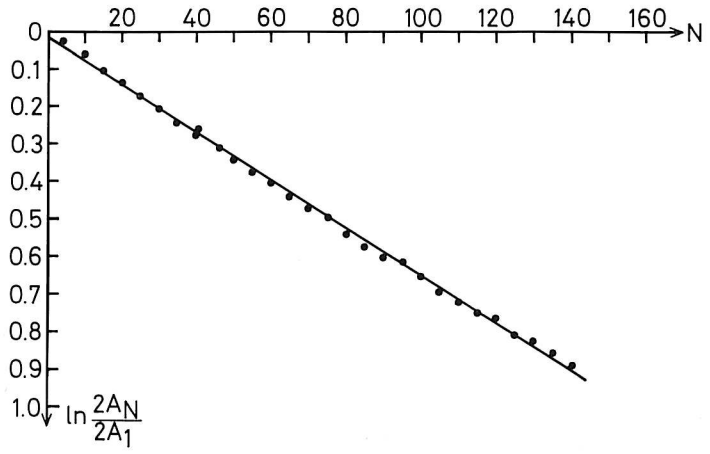

Figure 6.1. The relative logarithmic decrement of the first eigen mode in the first main direction.

Figure 6.1 shows that a straight line fit very well to the sampled points. The correlation is 0.9989. This is very satisfactory indeed and justify the chosen damping model. The damping ratio is found to be:

$$\zeta_1 = 0.108 \pm 0.002\,\%\ (95\,\%\, confidence)$$

It is seen that the monopile is very lightly damped. More than 30 oscillations could have been applied, but it is seen from figure 6.2 that convergence for the damping ratio as well as the variance has already almost been obtained. The variance may mainly be due to the visual determination of the oscillation values. The weakly decreasing damping ratio may be due to the fact that the decrease in the amplitudes became more and more difficult to measure as the amplitudes became smaller. Another reason might be that the damping depends on the level of oscillation.

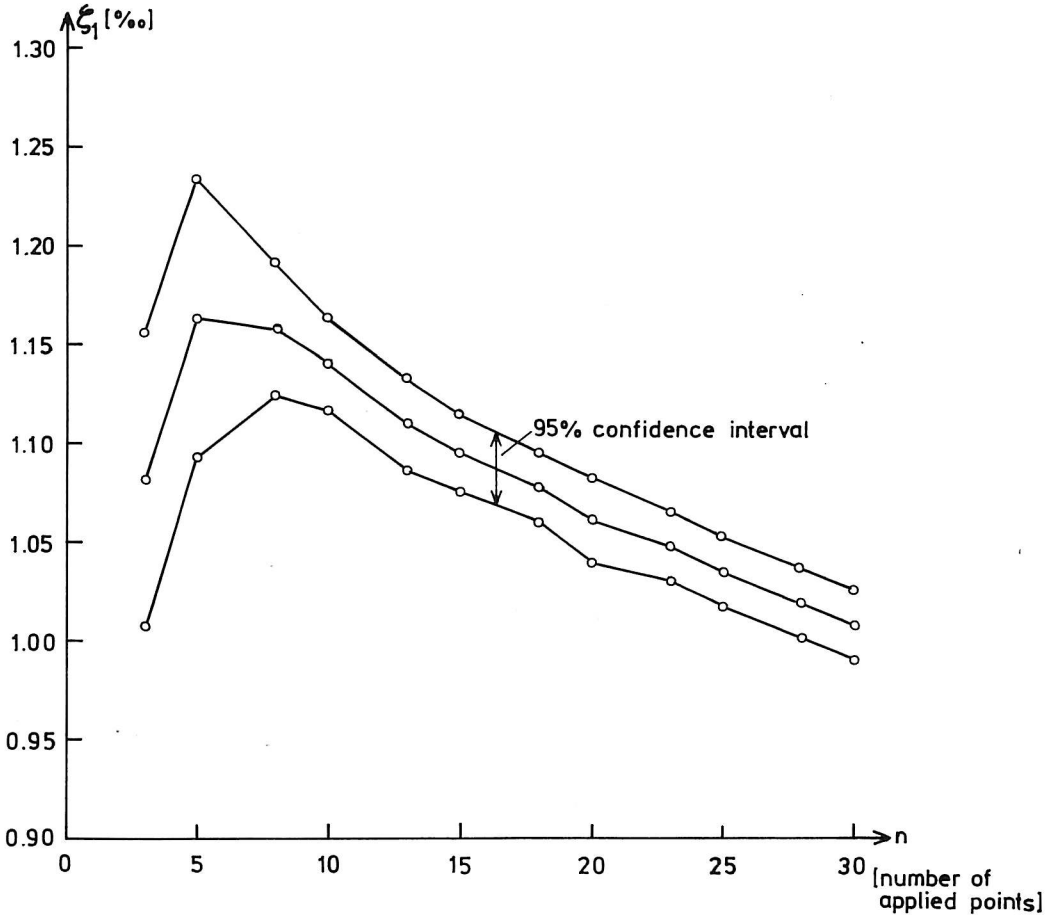

Figure 6.2. The damping ratio and the 95 % confidence interval as a function of the number of applied points.

6.2 Peak values of transfer functions

The damping ratio can as shown in chapter 4 in be determined from the peak values of the transfer functions. However, the overall standing problem is the estimation of the correct peak values. This is only possible if the frequency resolution is sufficient in the FFT analysis. Insufficient frequency resolution means that the estimated peaks are too small and consequently the estimated damping ratios too large.

	white noise acc. mass 1	periodic noise acc. mass 1	periodic noise acc. mass 2
ζ_1	0.0090	0.0034	0.0041
ζ_2	0.0066	0.0040	0.0056

Table 6.1. Damping ratios identified from the peak values of the transfer functions.

The identified damping ratios are shown in table 6.1. Compared with each other the results show a significant deviation. The damping ratios corresponding to the first eigen mode are seen to be considerable higher than the one found from the free vibration. This is without doubt due to insufficient frequency resolution which have led to unreliable estimates of the peak values.

6.3 Identification from peak shapes.

The damping ratios are here found from the shape of the resonance peaks of the transfer functions. The damping ratio is determined as the squared value which is the slope of a straight line assuming the model is correct. The method is described in chapter 4. The transfer functions are determined using FFT analysis.

Analysis	f_i Hz	ζ_i	Γ_{ζ^2} %
Periodic noise mass 1 displacement	1.117 7.203	0.014 0.0012	70-80 95-125
Periodic noise mass 1 acceleration	1.105 7.190	0.0029 0.0027	75 100
White noise mass 1 displacement	1.116	0.008	60-70
White noise mass 1 acceleration	1.089 7.168	0.0175 0.0052	175 70
White noise mass 1 acceleration	1.113 7.180	0.011 0.0024	145 72

Table 6.2. Estimated eigen frequencies and damping ratios using the peak shape method for various FFT results. Γ_{ζ^2} is the variation coefficient of ζ^2.

Table 6.2 shows the results using the peak shape method. The variation of the estimated damping ratio is given by the variation coefficient of the squared value of

the damping ratio. The results are seen to be very unreliable indeed. The variation coefficient has at least a magnitude of 60-70 %. This is very unsatisfactory and indicates some kind of error. The estimated damping ratio shows a great variation depending on which FFT result was applied in the analysis. The results are useless.

The cause to the unreliable results are probably insufficient frequency resolution. Furthermore, more averaging should probably have been made in the FFT analysis.

The fact that the identified damping ratios of the first mode are greater than the value found from the free vibration supports the explanation regarding frequency resolution. It should be mentioned that the spectrum analyser, HP3582A did not provide a higher resolution.

6.3 The circle fit method.

Transfer and phase functions were obtained from measured mass acceleration and base displacement. These functions were transformed to mobility data also given by transfer and phase functions ("mobility" refers to mass velocity relative to base acceleration). Finally the new transfer and phase functions were transformed to a real and imaginary function. This transformation included removal of the base movement which was contained in the measured response signal of the masses, refer to chapter 4.1 .

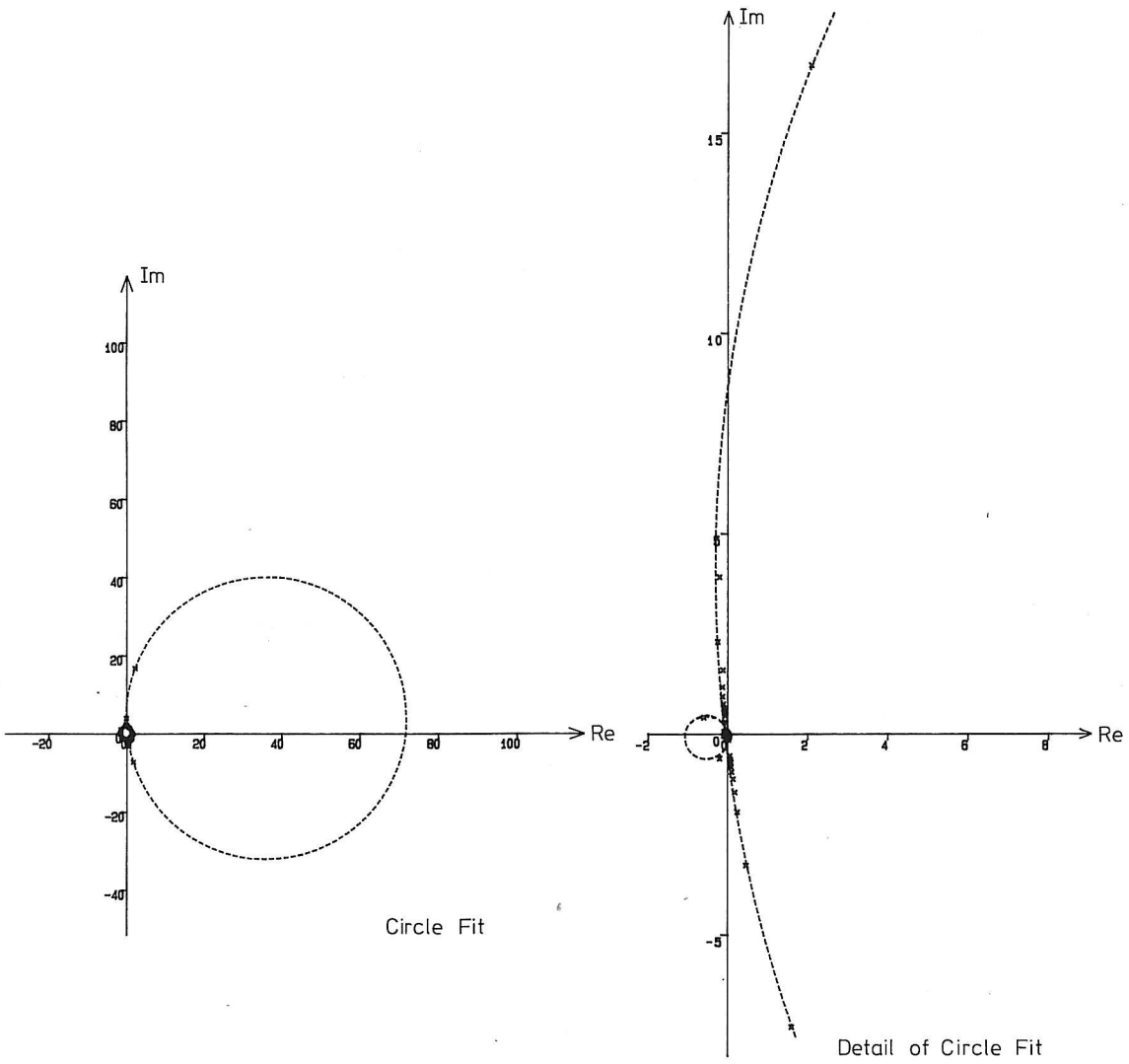

Figure 6.3. Circle fit. The acceleration of mass 1 with periodic noise excitation. Re refers to $Re[\frac{\dot{X}_1}{\dot{X}_b}]$ and Im refers to $Im[\frac{\dot{X}_1}{\dot{X}_b}]$.

The circle fit method was now applied to obtain information about the damping ratios. An example of a circle fit is shown in figure 6.3 based on data obtained from periodic noise excitation. The radius and the centre of the two circles were estimated from the mobility data. The circle in the right half plane corresponds to the first mode and the circle in the left half plane corresponds to the second mode. At first glance the two circle fits seem to be as expected according to the theory in /1/: A large circle in the right half plane and a small circle in the left half plane, corresponding to a lightly damped two degrees of freedom system with clearly separated eigen frequencies. However, the damping estimation gives more

or less absurd results.

Table 6.3 shows the results of the circle fit estimation. A different number of data points has been applied to estimate the circle and the parameters. The applied points were those centred around the resonance frequency.

Number of points	Circle fit error	f_i Hz	ζ_i	σ_ζ
21	0.0081	1.1208	-9.5049	0.5523
10	0.0113	1.1208	-2.1745	0.2922
3	0.0157	1.1102	0.0021	0.0008
21	0.0673	7.0823	0.0027	0.0107

Table 6.3. Estimated parameters from circle fit. Data:Acceleration of mass 1 with periodic noise excitation. σ : standard deviation.

It is seen that sensible results are obtained only for three points of the first mode. In this case the damping ratio is positive and the estimated eigen frequency corresponds to previous estimates obtained by other methods, see chapter 5. The estimated damping ratio becomes:

$$\zeta_1 = 0.0021 \pm 0.0016\,\%\ (95\,\%\, confidence)$$

However, it is difficult to have much confidence in this result, because the estimated damping ratio depends very much upon the number of applied data points. Anyway, it can be noticed that the analysis of the free vibration gives an estimate within the given confidence interval.

Using all data points for the second mode the estimated damping ratio becomes :

$$\zeta_2 = 0.0027 \pm 0.0210\,\%\ (95\,\%\, confidence)$$

Obviously this is a very unreliable result and it is also seen from table 6.3 that the estimated eigen frequency is incorrect.

The main reason why the circle fit method fails is insufficient frequency resolution. It is seen from the figure that almost all data points are concentrated in an area of a

small part of the estimated circle. A better frequency resolution would have spread out the points on the circle, which would have given a better estimation of the circle and consequently the eigen frequencies and the damping ratios. Furthermore a better resolution would have meant a less distortion of the FFT results.

Another point should also be mentioned. The circle fit method is different from the other applied methods, because it uses the phase information. This is as well a strength as a weakness. It is a strength because there is additional information in the phase function which should be applied, but a weakness because the phase function is more uncertain than the transfer function. The phase function due to random signals is a little more unreliable because the phase function is not unambiguous for each given frequency. Furthermore, the phase function can easily be distorted by filters, amplifiers and integration of signals.

The problem about sufficient frequency resolution is characteristic for narrow banded response processes as it is the case for the response of lightly damped systems. The problem of the estimation of the damping ratio is illustrated in figure 6.4.

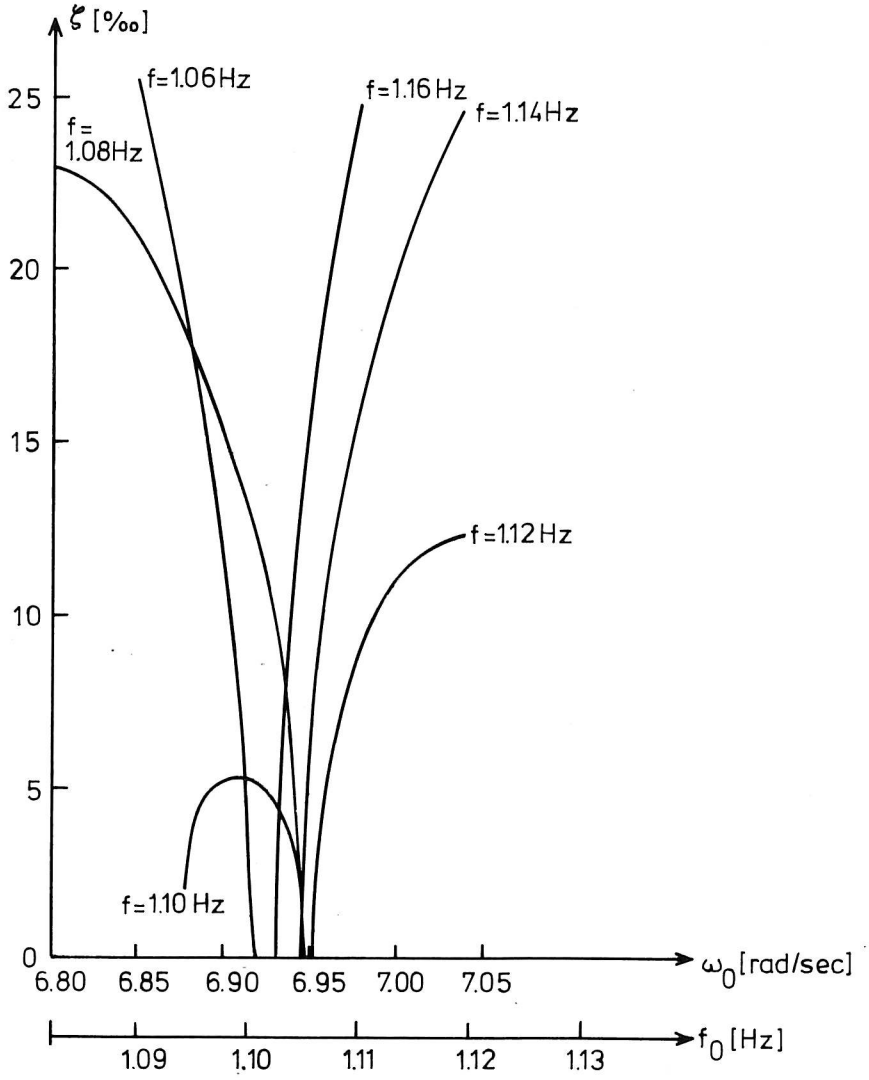

Figure 6.4. The damping ratio as a function of a given eigen frequency for different data points around the first resonance peak. Data: Transfer function of the acceleration of mass 1 with periodic noise excitation.

Figure 6.4 shows for each data point of the transfer function how the damping ratio depends on the given eigen frequency. A theoretical transfer function would naturally have given one intersection point of all the curves corresponding to a given damping ratio. This is not the case for the experimentally determined transfer function, and it is understood that a small distortion of the estimated eigen frequency easily leads to wrong damping estimates which may become negative.

The relation between damping ratio and eigen frequency is most sensitive for lightly damped systems. Higher damping ratio will give less steep curves. For lightly damped systems the figure shows that simultaneous estimation of eigen frequencies and damping ratios might result in less sensitive damping estimates.

In the present case it can be concluded that the circle fit method is relative vulnerable towards the estimation of the eigen frequencies when the system is lightly damped. It is clear that a more effective eigen frequency estimation is necessary if the circle fit method is supposed to be applied for lightly damped systems.

6.4 Estimation using ARMA models

ARMA models have been applied to estimate the response spectrum of the mass displacements. Due to a white noise assumption the damping ratios have been estimated. As discussed in chapter 4 the white noise assumption is only an approximation because it is the white noise which is the base displacement while the force spectrum is described by a polynomial of order four which increases in the frequency interval.

As mentioned in chapter 4 the appropriate ARMA model of a vibrating system with n degree of freedom should be an ARMA(2n,2n-1) model assuming the white noise assumption is acceptable. The order of the ARMA model was increased until the relative residue was minimised and the system parameters had stabilized.

The damping ratios were estimated using the peak shape method on the amplitude spectrum obtained from the ARMA model. This procedure gave no contribution to estimation error because the ARMA model order corresponded to a vibrating system. The correlation of the peak shape method was consequently 1.00.

In figure 6.5 and 6.6 the estimated damping ratios are shown as a function of the model order. The relative residue (the model error) is also shown. The expected model order was 4, but mainly due to the violated white noise the appropriate model order is seen to be an ARMA(14,13) model. The relative residue obtains it is minimum at 2n=14 and the damping ratios have become relative stabilized, especially the damping ratio for the second mode.

The reason why the damping ratio for the second mode stabilizes so quickly is probably the applied force spectrum. Due to the force spectral density increases with the frequency as a polynomial of order 4, the second mode is much stronger present in the response signal than the first one, which means that it is easier to identify, refer also to 4.4. The damping ratio of the first mode is seen to stabilize faster for the ARMA model of the response of mass 1 than the damping ratio determined from the response of mass 2. That may be due to the fact that the first mode is stronger represented in the response signal of mass 1 and consequently also better estimated in the ARMA model. It should be mentioned that the same tendency was recognized in the identification of the eigen frequencies.

The damping ratio corresponding to the ARMA(14,13) model is found to be:

Mass 1, sampling rate 40 Hz.

$$\zeta_1 = 0.00127$$

$$\zeta_2 = 0.00065$$

Mass 2, sampling rate 60 Hz.

$$\zeta_1 = 0.00256$$

$$\zeta_2 = 0.00045$$

The agreement between the results based on the response of the two masses does not seem to be satisfactory, however, the statistical uncertainty has not been estimated so this may be a wrong conclusion. It should be mentioned that the damping ratio of mode 1 estimated from the response of mass 1 has the same magnitude as the estimate found from the free vibration.

The most plausible explanation of the deviations is probably the one mentioned above regarding the presentation of the modes, but the failure of the white noise assumption does perhaps also lead to some kind of distortion of the resonance peaks and consequently the damping ratios. The sampling rate might also be of importance for the estimation results.

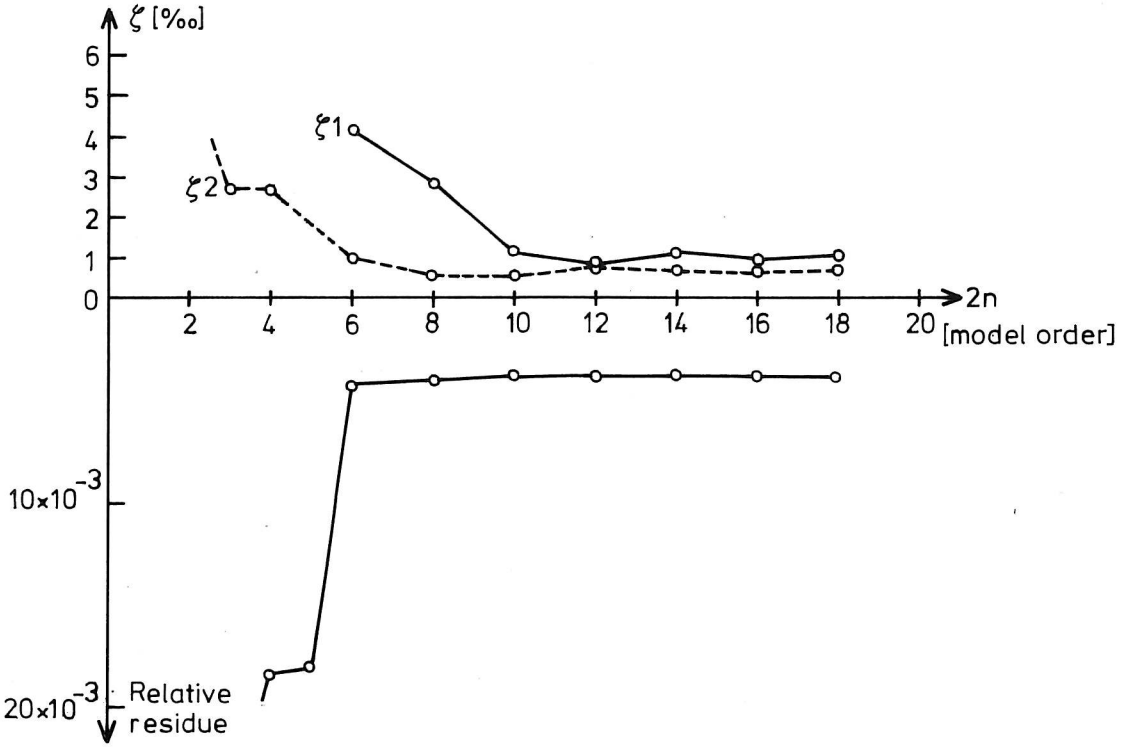

Figure 6.5. Convergence of the damping ratio and the relative residue. ARMA model based on the displacement of mass 1, sampling rate 40 Hz.

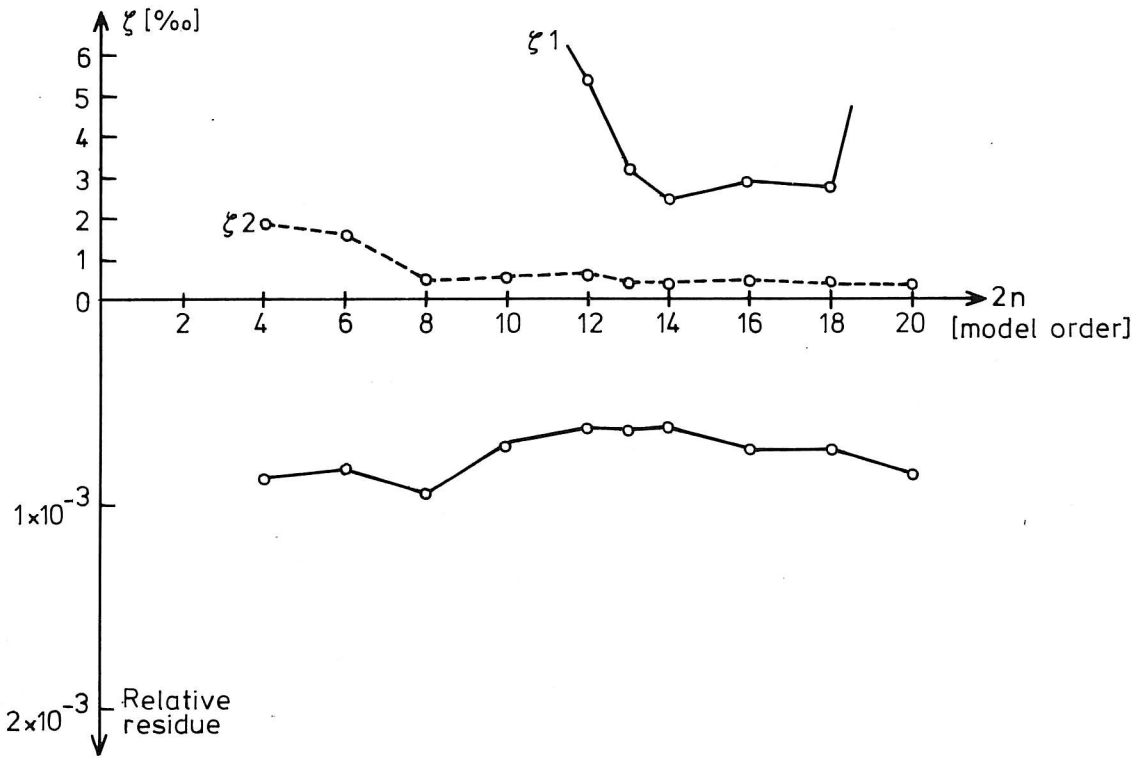

Figure 6.6. Convergence of the damping ratio and the relative residue. ARMA model based on the displacement of mass 2, sampling rate 60 Hz.

6.5 The effect of fatigue.

At a certain stage of the experiment a sudden decrease in the eigen frequencies was noticed. At the end of the experiment the explanation was found. A large fatigue crack had developed just above the weld, see figure 2.9. The crack had run more than half the way through the box profile.

After the cracked had been recognized, a free vibration was performed in the direction of each of the two main directions. This gave a new set of eigen frequencies and damping ratios.

As mentioned in chapter 5 the eigen frequencies had decreased from 1.10 and 7.19 Hz to 0.93 and 6.56 Hz respectively for the modes in the first main direction. The damping ratio for the first mode was found to have increased from :

$$\zeta_1 = 0.101 \pm 0.002\,\%\ (95\,\%\, confidence)$$

to:

$$\zeta_1 = 0.559 \pm 0.016\,\%\ (95\,\%\, confidence)$$

The relative logarithmic decrement was applied to estimate the damping ratios, see figure 6.7. The free vibration in the second main direction gave for the first mode the damping ratio:

$$\zeta_1 = 0.168 \pm 0.004\,\%\ (95\,\%\, confidence)$$

corresponding to the eigen frequency, 1.68 Hz.

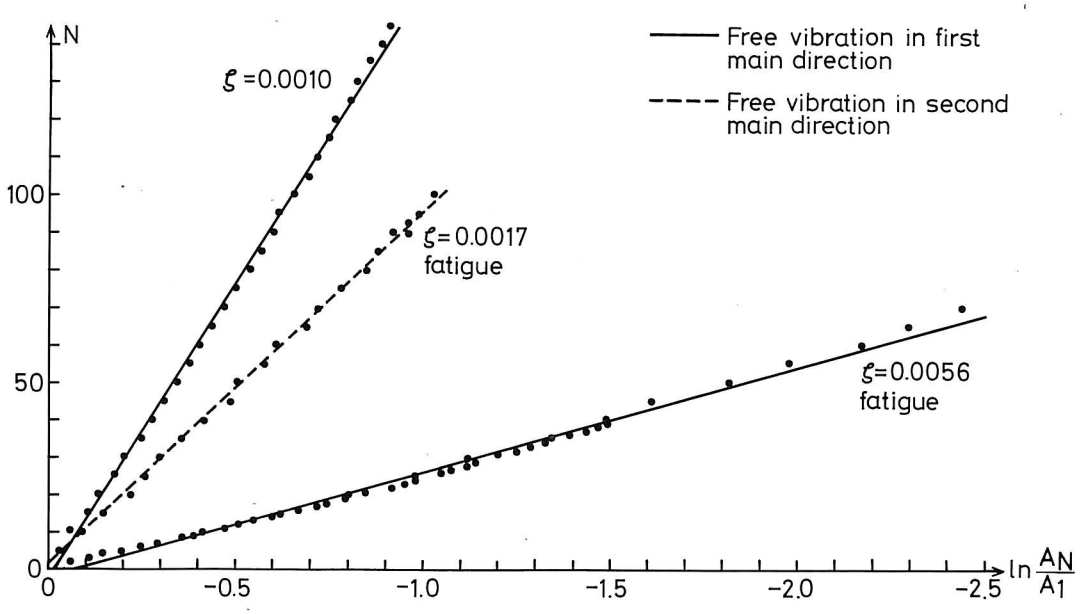

Figure 6.7. The damping estimation given by the logarithmic decrement before and after fatigue.

It is seen that while the first eigen frequency dropped 15 % the corresponding damping ratio increased almost 600 %. This shows that the damping ratio may be applied to indicate fatigue.

It is seen from the figure that the estimation of the damping ratio also shows a great correlation for the data after fatigue has been recognized. Still the damping model seems adequate even though it is difficult to relate the open fatigue crack with a viscous damping mechanism. The point may be that the damping is still small and therefore easy to fit to any model.

6.7 Conclusion

The estimation of the damping ratio has shown that it is a quantity which is very difficult to identify. While the deviations between the estimated eigen frequencies are less than 1%, the estimation of the damping ratio gives deviations which are often larger than 100%. This is very unsatisfactory. However, the estimation from the free vibration seems to give very reliable results within a 95 % confidence interval of 2-3 %. This is indeed a very reliable estimation superior to all other methods. The damping ratio of the first eigen mode was found to be 0.001. The fact that the damping ratio is very small is the reason why some of the estimation methods completely fail or give very unreliable results.

Besides, the damping estimate obtained from the free vibration by the logarithmic decrement, the estimates obtained from the ARMA models are also considered relatively reliable. One of the estimates obtained from the ARMA model corresponds very well with the estimate from the free vibration. As a fact the method does show some possibilities whereas the FFT analysis has failed completely. The failure of the FFT analysis is without doubt due to insufficient frequency resolution and perhaps to the numbers of averages. This have caused very uncertain damping estimates which were also too high due to the insufficient resolution. In the future higher demands must be made when FFT analysis is used as a tool.

Finally it should be mention the results of the experiment have shown that the damping ratio can be sensitive with respect to the development of a fatigue crack.

7 DETERMINATION OF MODE SHAPES

The two mode shapes corresponding to the two lowest eigen frequencies in the main direction have been estimated. They were determined directly by measurement with a sinusoidal excitation and further more they were estimated indirectly from the determined transfer functions. Finally the mode shapes determined from the experimental results have been compared with computed mode shapes from theoretical models.

It was possible to measure the lowest mode shapes because the model was a simple one. This was simply done by tuning the input frequency until resonance was reached. The resonance frequency was determined by watching the response of the model using eyes and ears. This resonance determination was sufficient because the construction was extremely lightly damped. The mode shapes were measured with four accelerometers placed along the monopile. Besides, the measured displacement at four points the node in the second mode shape was found. This was done by moving the accelerometers until no response was measured. The measured mode shapes are shown in figure 7.1. A polynomial of order 4 has been fitted to the measured results to obtain a complete mode shape. The results from the finite element model are also shown.

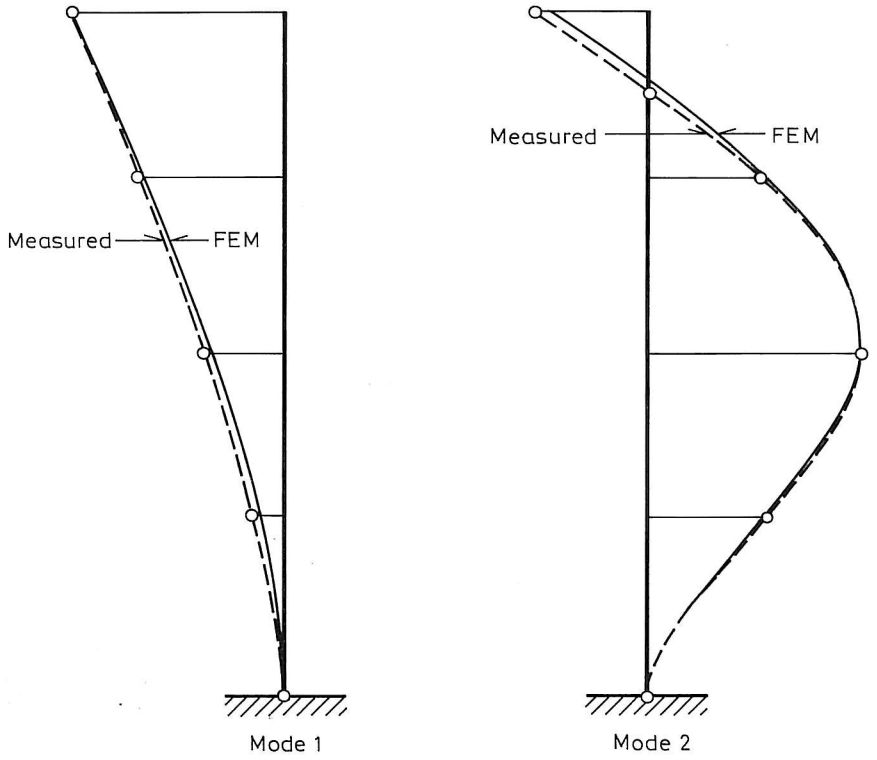

Figure 7.1. Measured and computed(FEM model) mode shapes corresponding to 1.11 Hz and 7.20 Hz.

The mode shapes were also determined indirectly from the measured transfer functions. If the excitation force had only been one force at mass 1 or 2 at a time it would have been easy to compute the mode shapes directly from the peak values of the transfer functions. However, due to the assumed orthogonallity condition and known masses it was possible to compute the mode shapes and the damping ratios from a system of equations for the transfer functions.

As mentioned in chapter 4 the equations to solve are shown to be:

$$\begin{pmatrix} 2D_{11} & -2D_{12} & 0 \\ 2D_{21} & 2D_{22} & 0 \\ \frac{M_2}{M_1}2D_{12} & -2D_{12} & \frac{-(M2+M_2^2)}{M_1} \end{pmatrix} \begin{pmatrix} \zeta_1 \\ \zeta_2 \\ \Phi_{12}^2 \end{pmatrix} = \begin{pmatrix} 1 \\ 1 \\ 0 \end{pmatrix} \tag{4.22}$$

where D_{ij} is the dynamic amplification for the displacement of mass i at the eigen frequency no. j. The masses M_1 and M_2 are here lumped masses. In general the lumped mass distribution has been found so that the orthogonallity conditions were satisfied. From the data obtained from the FFT results for the displacement response with periodic noise excctation one gets the results shown in table 7.1.

Together with the mode shapes determined from measurements, the results from two theoretical computations based on a lumped mass model with 2 degrees of freedom and a finite element model are also shown . The assumptions and the general results of the two models are given in /4/. The results from the finite element model are also shown in figure 7.1.

	Measured (sinusoidal)	Peak values (periodic noise)	FEM model	Lumped mass model
$\overline{\Phi}_1$	1.00 0.38	1.00 0.38	1.00 0.34	1.00 0.32
$\overline{\Phi}_2$	-0.53 1.00	-0.46 1.00	-0.48 1.00	-0.39 1.00

Table 7.1. Comparison of the estimated mode shapes.

Table 7.1 shows a good agreement between the results. The deviations between the determined mode shapes are greatest for the second mode. The mode shapes determined from peak values respectively FEM model give here a deviation about 13 %. The lumped mass model gives the purest agreement with the measured results. The lumped mass distribution chosen in the lumped mass model and the peak value model were the same but the results do not agree very well.

The results from the FEM model are also shown in figure 7.1. It is seen that the deviations for the first mode indicate that the clamped beam assumption can be the cause to some of the deviation. This potential model error may be due to the development of the fatigue crack. This explanation agrees with the fact that the FEM model gave a first eigen frequency of 1.15 Hz while the measured was 1.11 Hz. Furthermore, the test after the mode shape test definitely gave a fatigue crack. This was noticed as a drop in the eigen frequency to about 0.9 Hz. So it can be concluded that the monopile model during the experiment had some kind of defect in the welded area which could be the cause of a smaller stiffness than expected.

This fatigue explanation is perhaps also some of the explanation of the difference between the results from the peak value determination and the measurements. However, insufficient frequency resolution is just as likely an explanation. Finally it must be remembered that the measured results also may have contained some error. For instance it was noticed that it was difficult to tune the input frequency exactly.

8 ESTIMATION OF THE TRANSFER FUNCTIONS

The dynamic parameters of the monopile model were estimated in chapter 5,6 and 7. Given these parameters the purpose of this chapter is to compare the theoretical and experimental transfer functions. However, before this is done, the mass and stiffness matrix of the model are investigated.

8.1 Mass and stiffness modelling

The monopile is still considered as a two degrees of freedom system. The purpose is now to obtain information about the mass and stiffness matrices from the measured mode shapes which were presented in chapter 7.

It is assumed that orthogonallity conditions holds:

$$\underline{\underline{\tilde{\Phi}}}^T \underline{\underline{M}} \underline{\underline{\tilde{\Phi}}} = \underline{\underline{I}} \tag{4.9}$$

From (4.9) it is possible to estimate a lumped mass model as well as the weighted mode shape matrix. The weighted mode shapes are given by the relation :

$$\underline{\tilde{\Phi}}_{(i)} = \frac{1}{\sqrt{M_{ii}}} \underline{\Phi}_{(i)} \tag{8.1}$$

From (4.9) and (8.1) one obtains the relations:

$$\frac{M_1}{M_2} = -\frac{\Phi_{22}\Phi_{12}}{\Phi_{21}\Phi_{11}} \tag{8.2}$$

$$\frac{\sqrt{m_{22}}}{\sqrt{m_{11}}} = \sqrt{\frac{-M_1\Phi_{21}^2 + M_2\Phi_{22}^2}{M_1\Phi_{11}^2 + M_2\Phi_{12}^2}} \tag{8.3}$$

Now, if (8.2) is inserted in (8.3) one obtains:

$$\frac{\sqrt{m_{22}}}{\sqrt{m_{11}}} = \sqrt{\frac{-\Phi_{22}\Phi_{12}\Phi_{21}/\Phi_{11} + \Phi_{22}^2}{\Phi_{22}\Phi_{11}\Phi_{11}/\Phi_{21} + \Phi_{12}^2}} \tag{8.4}$$

From (8.4) it is possible to obtain information about the ratio of the modal masses. From the present measured mode shapes (8.2) and (8.4) give the results :

$$\frac{M_1}{M_2} = 0.7170 \tag{8.5}$$

$$\frac{\sqrt{m_{22}}}{\sqrt{m_{11}}} = 1.1810 \tag{8.6}$$

From the orthogonallity conditions, (4.9) and (8.5) the mass matrix can now be found by iteration. The final result becomes:

$$\overline{\overline{M}} = \begin{pmatrix} 25.56 & 0 \\ 0 & 35.65 \end{pmatrix} [kg] \tag{8.7}$$

where the orthogonallity is given by:

$$\overline{\overline{\Phi}}^T \overline{\overline{M}} \overline{\overline{\Phi}} = \begin{pmatrix} 30.7100 & -0.0002 \\ 0.0002 & 42.8300 \end{pmatrix} [kg] \tag{8.8}$$

and the weighted mode shape matrix by :

$$\overline{\overline{\Phi}} = \begin{pmatrix} 0.1805 & 0.0810 \\ 0.0686 & -0.1528 \end{pmatrix} [kg^{-\frac{1}{2}}] \tag{8.9}$$

Now it is possible to find the stiffness matrix of the 2 degrees of freedom system due to the relations:

$$\overline{\overline{\Phi}}^T \overline{\overline{K}} \overline{\overline{\Phi}} = (\omega_i^2)$$

$$\overline{\overline{K}} = \overline{\overline{\Phi}}^{-T} (\omega_i^2) \overline{\overline{\Phi}}^{-1}$$

$$\overline{\overline{K}} = \overline{\overline{M}} \overline{\overline{\Phi}} (\omega_i^2) \overline{\overline{\Phi}}^T \overline{\overline{M}} \tag{8.10}$$

Assuming the eigen frequencies to be 1.11 hz and 7.19 hz (transformed to rad/sec) one obtains the stiffness matrix for the two degrees of freedom system :

$$\overline{\overline{K}} = \begin{pmatrix} 9783.4 & -22468.3 \\ -22468.3 & 60851.1 \end{pmatrix} [N/m] \tag{8.11}$$

This result can be compared with the stiffness matrix obtained from the flexibility matrix of the box profile of the monopile:

$$\overline{\overline{K}} = \begin{pmatrix} 8955.0 & -22387.5 \\ -22387.0 & 71640.0 \end{pmatrix} [N/m] \tag{8.12}$$

This corresponds to the deviations:

$$\overline{\overline{\Delta}} = \begin{pmatrix} 8.5 & 0.4 \\ 0.4 & 17.7 \end{pmatrix} [\%] \tag{8.13}$$

The deviations are seen to be rather small and the result must be said to be very satisfactory. This indicates that the two degrees of freedom assumption was reasonable which it was also expected to be.

8.2 Transfer function models

The expression for the transfer function of two degrees of freedom system was found in chapter 4 to be given by:

$$\frac{X_1}{\ddot{X}_b} = -\frac{K_{11}}{{\omega_1}^2 - \omega^2 + 2\omega_1\omega\zeta_1 i} - \frac{K_{12}}{\omega_2^2 - \omega^2 + 2\omega_2\omega\zeta_2 i} \tag{3.14a}$$

$$\frac{X_2}{\ddot{X}_b} = -\frac{K_{21}}{{\omega_1}^2 - \omega^2 + 2\omega_1\omega\zeta_1 i} - \frac{K_{22}}{\omega_2^2 - \omega^2 + 2\omega_2\omega\zeta_2 i} \tag{3.14b}$$

where:

$$K_{11} = \Phi_{11}^2 M_1 + \Phi_{11}\Phi_{12} M_2$$
$$K_{12} = \Phi_{21}^2 M_1 + \Phi_{22}\Phi_{21} M_2$$
$$K_{21} = \Phi_{12}\Phi_{11} M_1 + \Phi_{12}^2 M_2$$
$$K_{22} = \Phi_{21}\Phi_{22} M_1 + \Phi_{22}^2 M_2$$

The theoretical transfer functions can now be computed with the knowledge of the mass matrix and the weighted mode shapes which were found in chapter 8.1. Values for the eigen frequencies and the damping ratios are also needed in the expression of the theoretical transfer functions. The following values have been used:

$$f_1 = 1.1054; hz$$
$$f_2 = 7.1921; hz$$
$$\zeta_1 = 0.00127$$
$$\zeta_2 = 0.00065$$

These values correspond to the ARMA(14,13) model used in chapter 5 and 6.

With these input parameters the theoretical transfer functions have been compared with the results of the FFT analyses. The transfer function is here defined as the mass response (including measured base movement) relative to the base displacement.

The transfer functions for the displacement of mass 1 and mass 2 are shown in figure 8.1a and 8.1b. Even though the experimental results show a large scattering the agreement is reasonable. One reason to the scattering could be the use of the periodic noise excitation source because this provides only a discrete input spectrum as mentioned in chapter 2. This means that almost no excitation existed on certain frequencies which could lead to uncertain results, especially if the resolution also is not quite sufficient. Another cause to the scattering could be insufficient averaging. A large number of averages could be important because the response signal is displacement signal which is obtained by integration of acceleration signal. This integration may lead to uncertain results.

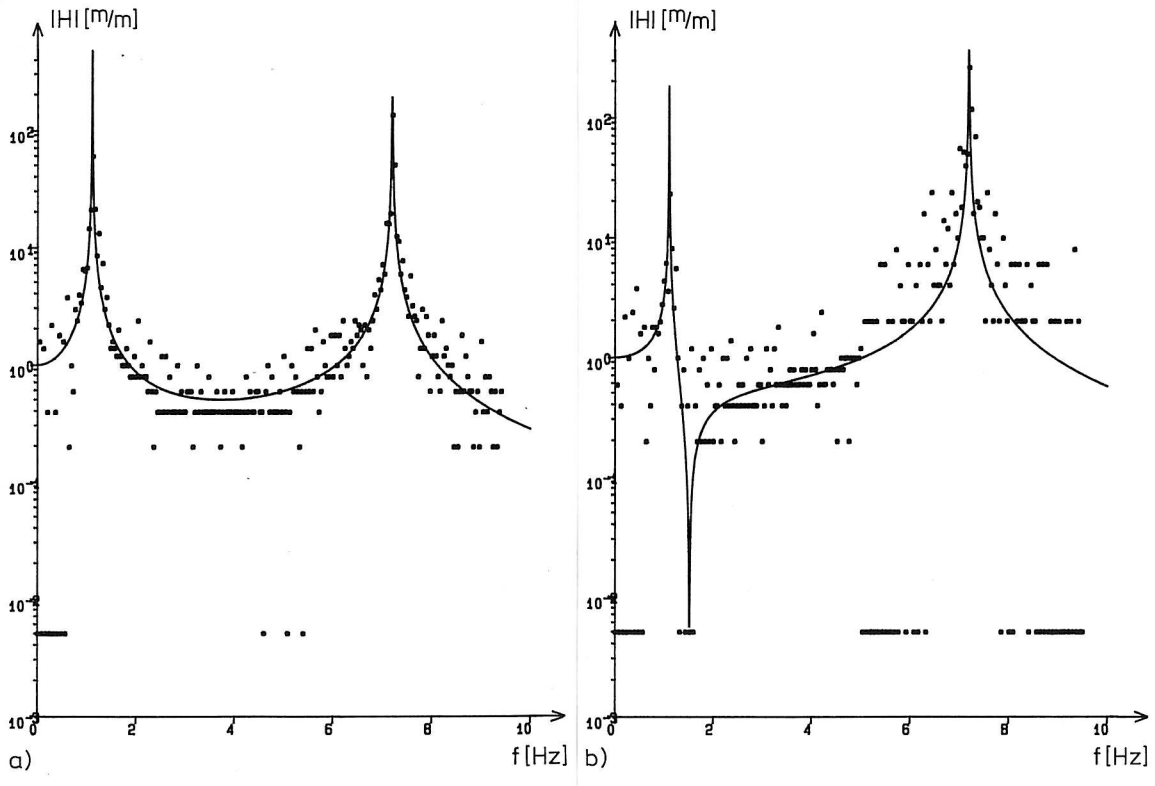

Figure 8.1. Transfer functions for displacement response with periodic noise excitation. a) Mass 1, b) mass 2. BW=0.04 hz. 8 averages.K_{11} =1.2742, K_{12} =-0.2735, K_{21} =0.4843 and K_{22} =0.5160

If one uses the acceleration response instead, the results become as shown in figure 8.2a and 8.2b. Here a better resolution has been used in the area from 0-2.5 hz. This leads to considerable reduction in the scattering in this interval compared with figure 8.1. Furthermore, the number of averages have been increased in the upper frequency domain but without any success. However, the results are better than those shown in figure 8.1. It is seen that the first resonance and the anti-resonance are modelled rather well. This can be due to the better resolution or the use of the acceleration response. The second resonance area does not show any convincing agreement between theory and experiment but at least the eigen frequency seems to be correct.

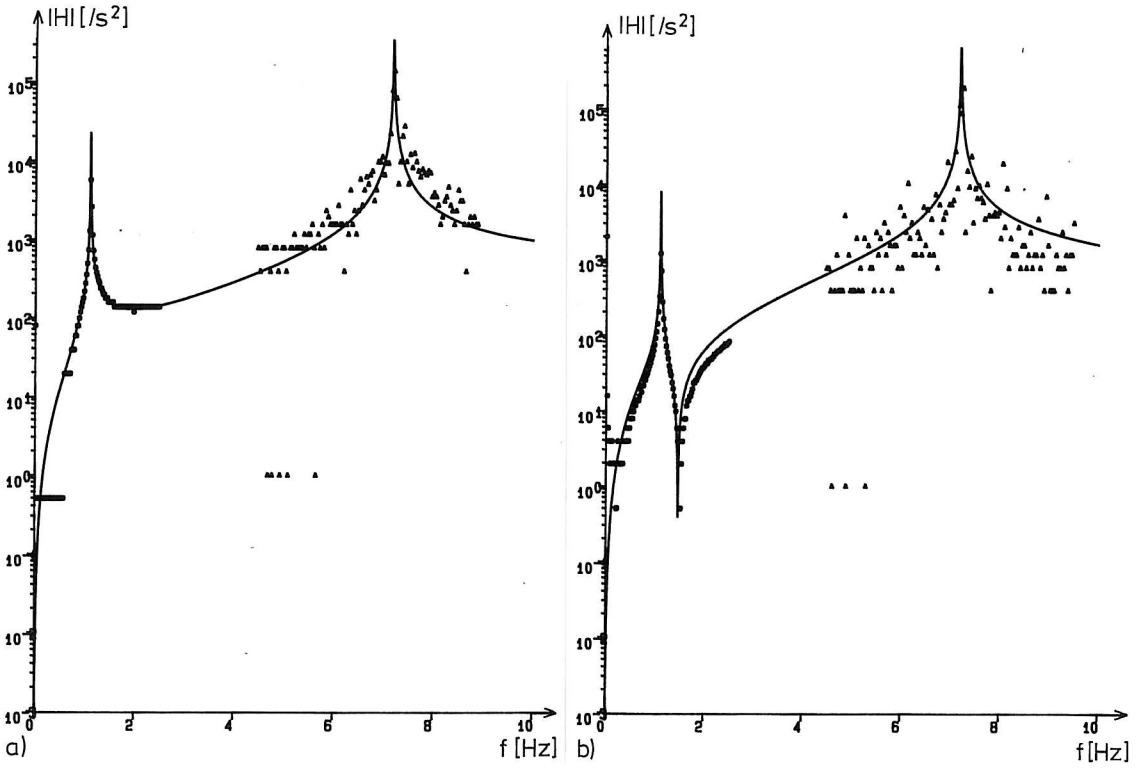

Figure 8.2. Transfer functions for the acceleration response with periodic noise excitation. a) Mass 1: 0-2.5 hz: BW=0.02 hz, 4 averages, 4.48-9.48 hz: BW=0.04 hz, 32 averages. b) Mass 2: 0-2.5 hz: BW=0.02 hz, 8 averages, 4.48-9.48 hz: BW=0.04 hz, 32 averages.K_{11} =1.2742, K_{12} =-0.2735, K_{12} =0.4830 and K_{22} =0.5160.

If the periodic noise excitation is replaced by white noise the result becomes as shown in figure 8.3. Theory and experiment agree very well indeed even though the resolution is much smaller, BW=0.06 hz. Furthermore in the upper frequency

domain the scattering is also much smaller than before. This seems to confirm that the periodic noise is the source to some of the scattering.

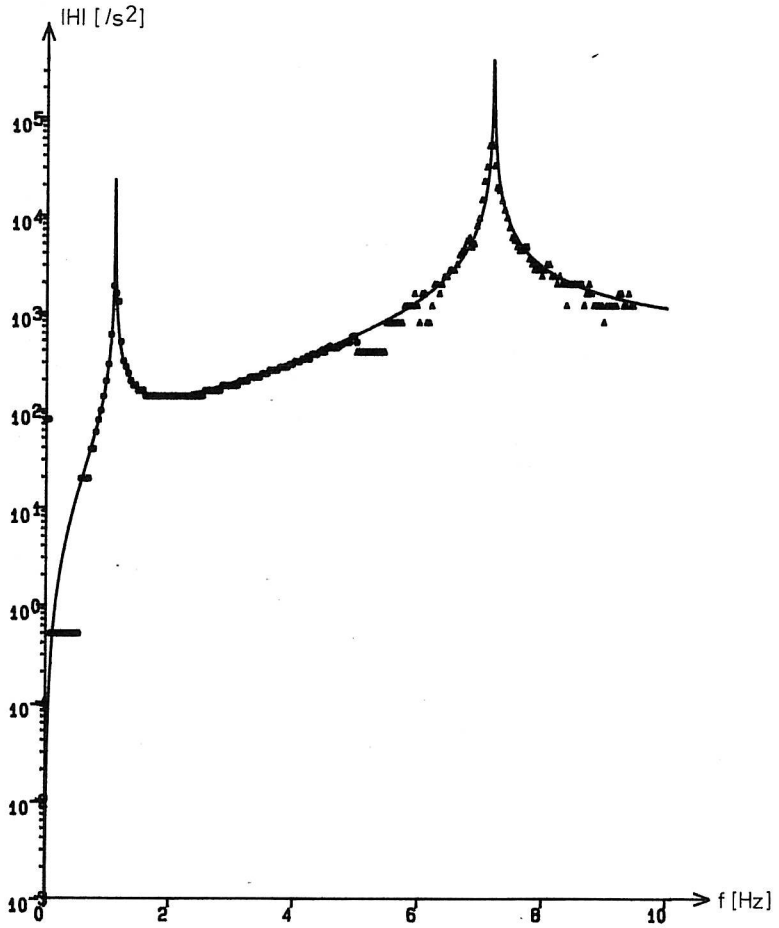

Figure 8.3. Transfer function for the acceleration of mass 1 with white noise excitation. BW=0.06 hz, 8 averages. K_{11} =1.2742, K_{12} =-0.2735, K_{21} =0.4830 and K_{22} =0.5160.

The characteristic phase function is shown in figure 8.4. 200 degrees have been added to the phase values. The results correspond to the data used in figure 8.3, but it is seen that the deviation between theory and experiment is more pronounced than in figure 8.3. Also the scattering seems to be bigger. The deviation is thought to be due to phase distortion in the measurement system (filters, transducers, amplifiers etc.). The scattering may be due to the averaging procedure in the spectrum analyser and the fact that random excitation does not give uniquely determined phase function. However, the agreement is acceptable with the excep-

tion of the low frequency region where the deviation is remarkable large. This may be due to a 360 degrees phase shift caused by phase distortion and noise in the signals.

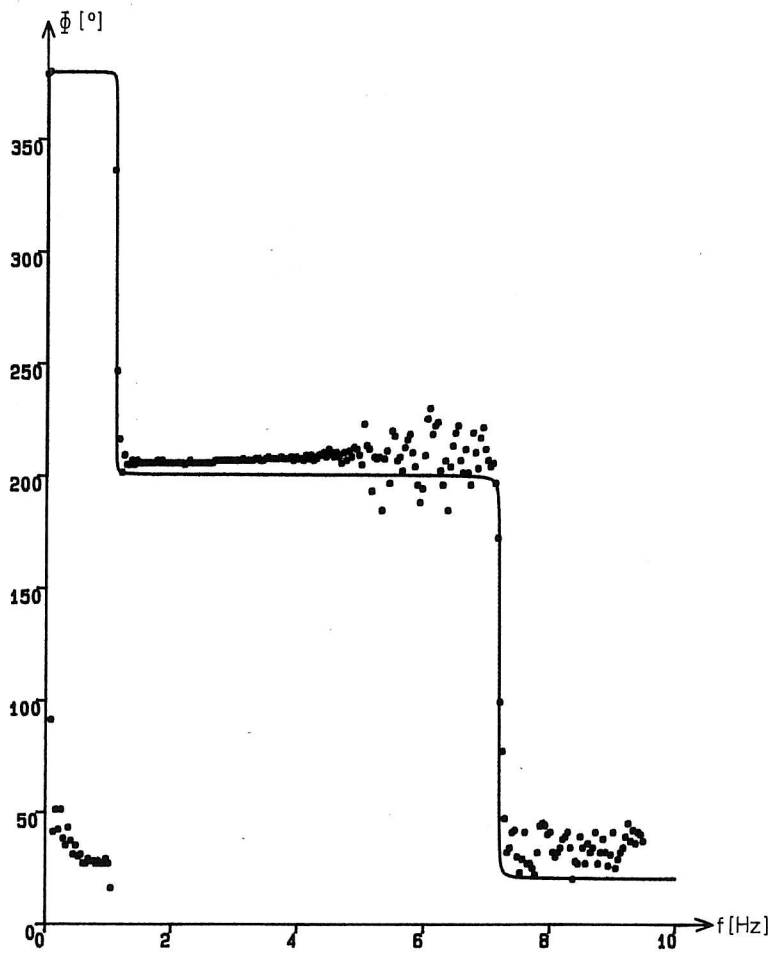

Figure 8.4 Phase function of the acceleration of mass 1 due to white noise excitation. 200 degrees added. BW=0.06 hz, 8 averages. K_{11} =1.2742, K_{12} =0.2735, K_{21} =0.4830 and K_{22} =0.5160.

8.3 Conclusion

In summary the comparisons between theory and experiment have given a good agreement. It has shown that the mass and stiffness relations can be identified quite well. Especially the transfer function has been estimated with success but it has to be remembered that the good agreement, which has been seen by the eye does not reveal the great uncertainty about the damping ratio estimated from the FFT data.

Finally it can be noticed that white noise excitation seems to give more reliable results than periodic noise excitation.

9.0 CONCLUSION

The report has presented the results and the obtained experience of the experiment with a monopile model which was excited by a shaker table.

The experience with respect to the shaker table excitation was that it provided a very effective excitation of the model. The interaction between the excitation system and the model was not without importance but seemed not to give rise to serious problems. However, the interaction has shown that sinusoidal excitation should be used with care because the interaction meant that the model more or less controlled the excitation about resonance. The consequence was none stationary signals. This was a problem which basic cause was that the model was very lightly damped.

The random noise excitation did mainly provide excitation of the second eigen mode because the force signal was much stronger around the second resonance. Experiments in the future should provide a modified force spectrum with the energy more equally distributed with respect to the frequency region of interest. It was also experienced that the use of the white noise source might give more reliable results than the periodic noise source.

Another experience was that a too high excitation level led to fatigue in the model. Especially the sinusoidal excitation was too strong. A lower excitation level should and could have been chosen. The fatigue caused a decrease in the eigen frequencies and the damping ratios about 20% and 600% respectively.

The eigen frequencies were estimated within 1% whereas the estimated damping ratios were very uncertain. The most reliable results gave a variation coefficient about 3% but the most common result was that the results deviated more than 100%. However, this deviation is thought to be due to insufficient frequency resolution and perhaps also averaging in the FFT analysis.

The very reliable damping estimates obtained from the free vibrations shows that the viscous damping model seems to be adequate. Even the damping estimates obtained after fatigue had occurred were found to be very reliable. This indicates that the damping model is rather flexible even when the damping mainly is due to a crack.

The identification methods which failed were all based on FFT results. Consequently it is difficult to make a fair comparison of the methods. However, it is clear that a lightly damped system always will make a high frequency resolution necessary if the damping ratio has to be estimated properly from FFT results. That is why the ARMA models have been shown some interest in this report and a certain amount of success has been obtained. Consequently it is also thought that future research should contain the use of ARMA models in system identification of vibrating systems.

The other estimation methods should not be rejected totally. Firstly, because

many other systems will be more damped and the frequency resolution demands will be less strict. Secondly, because the resolution problems in the present case were caused by the limitations of the applied frequency analyser. It is thought that a much better frequency analysis could have been performed applying a flexible FFT package available on a personal computer. However, the applied frequency analyser should not be totally underestimated because the analyser still will be an effective control tool during experiments.

The mode shapes and the transfer functions have also been estimated. The results have been very satisfactory. The agreement between theoretical and experimental results has been noticed to be rather well. The system of linear second order differential equations seems to provide an adequate model of the monopile model with respect to the mass and stiffness relations. It is not possible to make any conclusion about the damping model due to the uncertain results.

With respect to the future research the presented results have clearly shown that the damping of a system is very difficult to estimate. Consequently the future research must concentrate in the field of estimation of the damping and try to provide more information about the nature of the damping.

REFERENCES

/1/ Ewins, D.J. "Modal Testing: Theory and Practice" 1984,Research Studies Press Ltd.,England

/2/ Jensen, J.L. "Systemidentification 1: ARMA Models" 1988,To be published, Aalborg University Center, Denmark

/3/ Pandit, S.M. and S-M Wu. "Time Series and System Analysis with Applications" 1983, John Wiley & Sons Ltd., USA

/4/ NAG Liberary, version 1987 NAG Central Office Mayfield House 256 Banbury Road Oxford OX2 7DE, UK.

/5/ IMAGES 3D (Finite element program) Celestial Software Inc., 125 University Avenue, Berkley, CA 94710, USA

/6/ "Understanding the HP 3582A Spectrum Analyzer" Hewlett Packard, April 1978, USA

ENCLOSURE 1

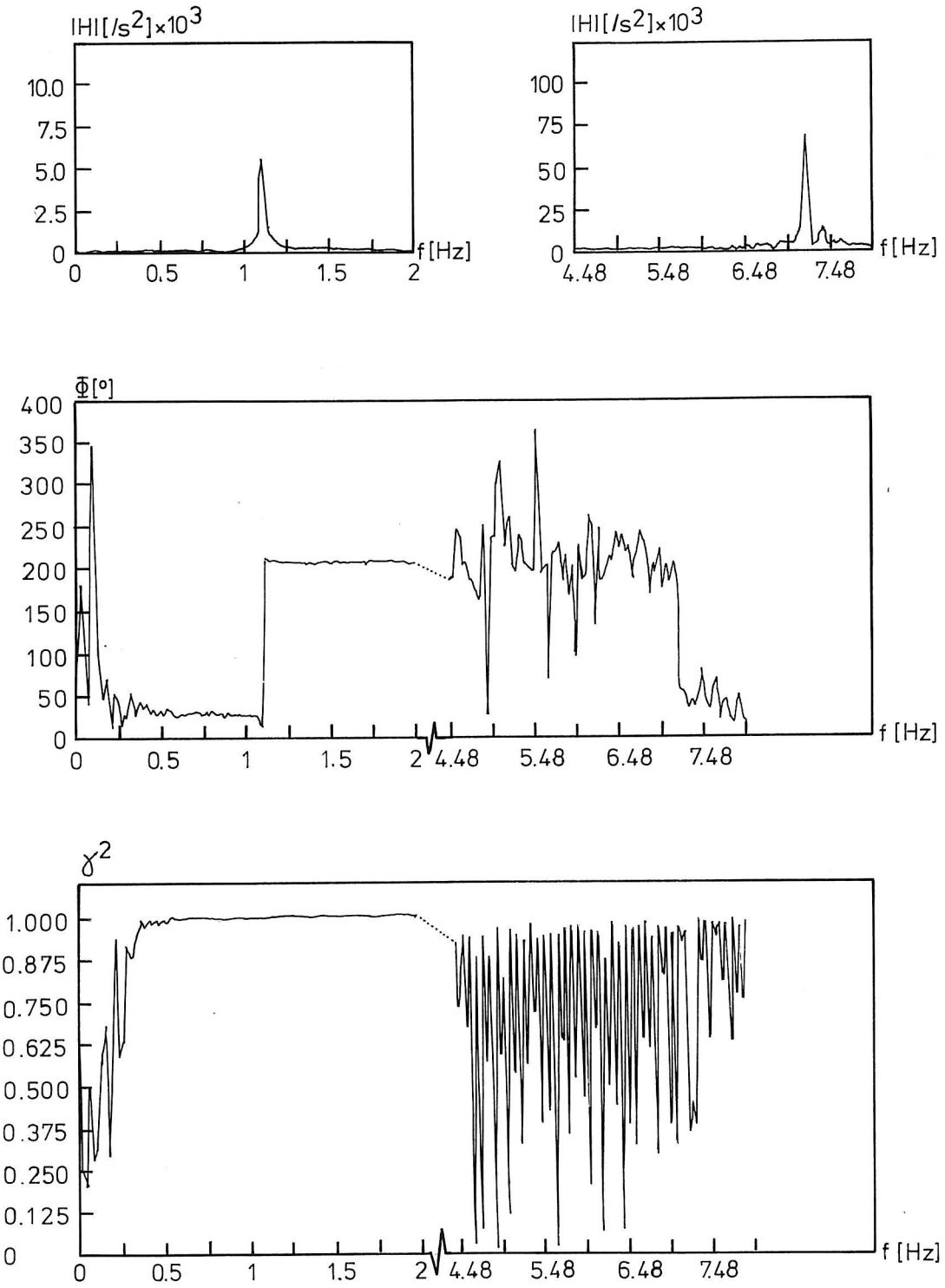

Response: Acceleration of mass 1. Excitation: Periodic noise. BW=0.02/0.04 hz. Number of averages: 4/32. Filter cutoff frequency of the noise signal: 3/12 hz.

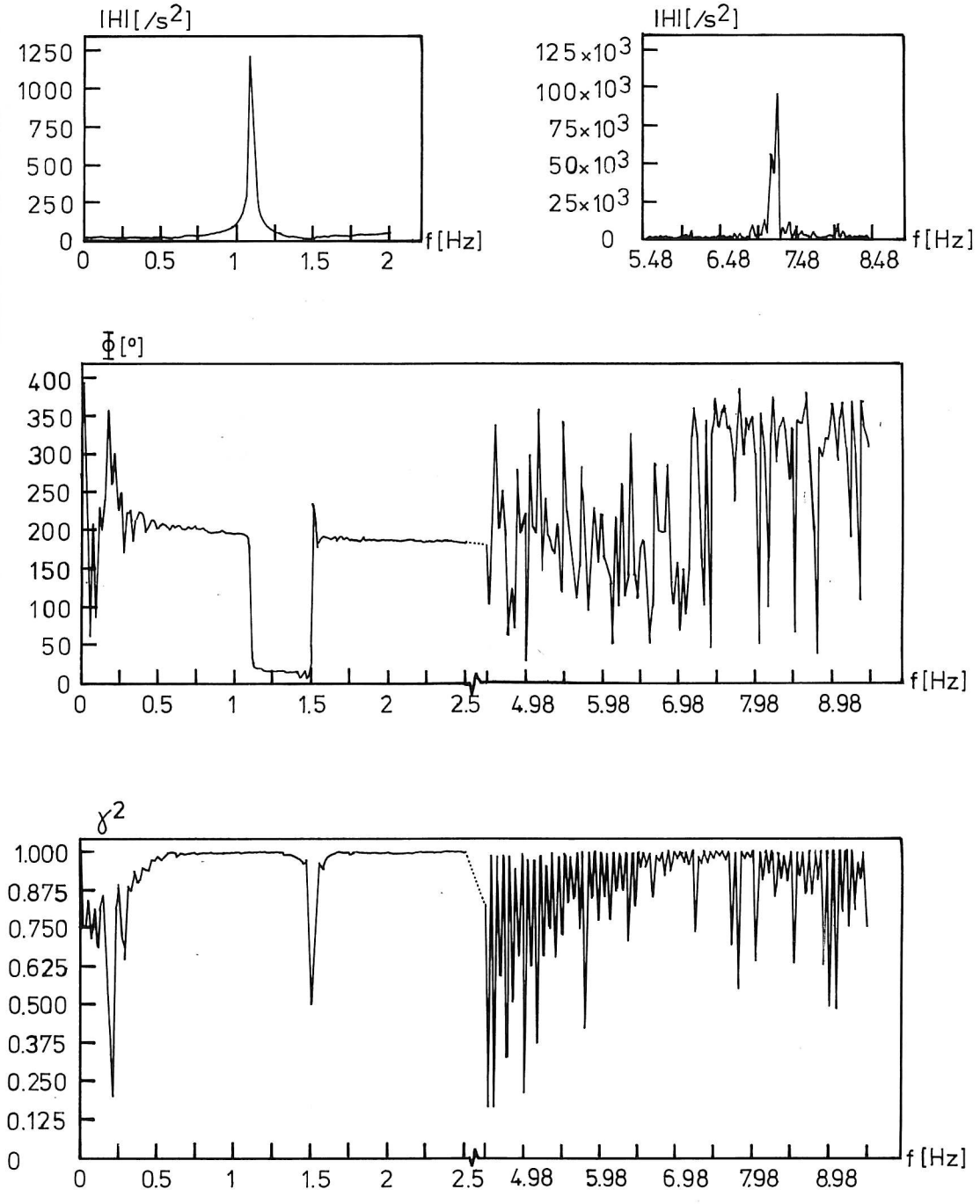

Response: Acceleration of mass 2. Excitation: Periodic noise. BW=0.02/0.04 hz. Number of averages: 8/32. Filter cutoff frequency of the noise signal: 3/12 hz.

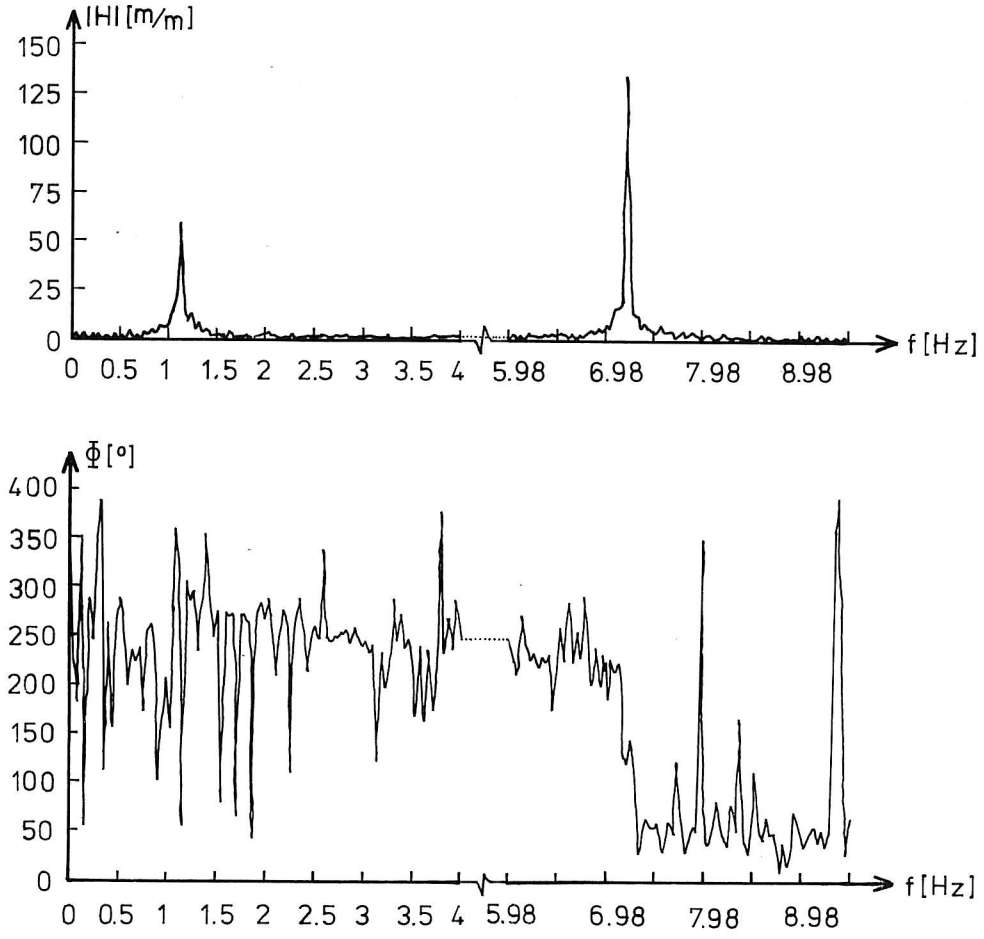

Response: Displacement of mass 1. Excitation: Periodic noise. BW=0.04 hz. Number of averages: 8. Filter cutoff frequency of the noise signal: 15 hz.

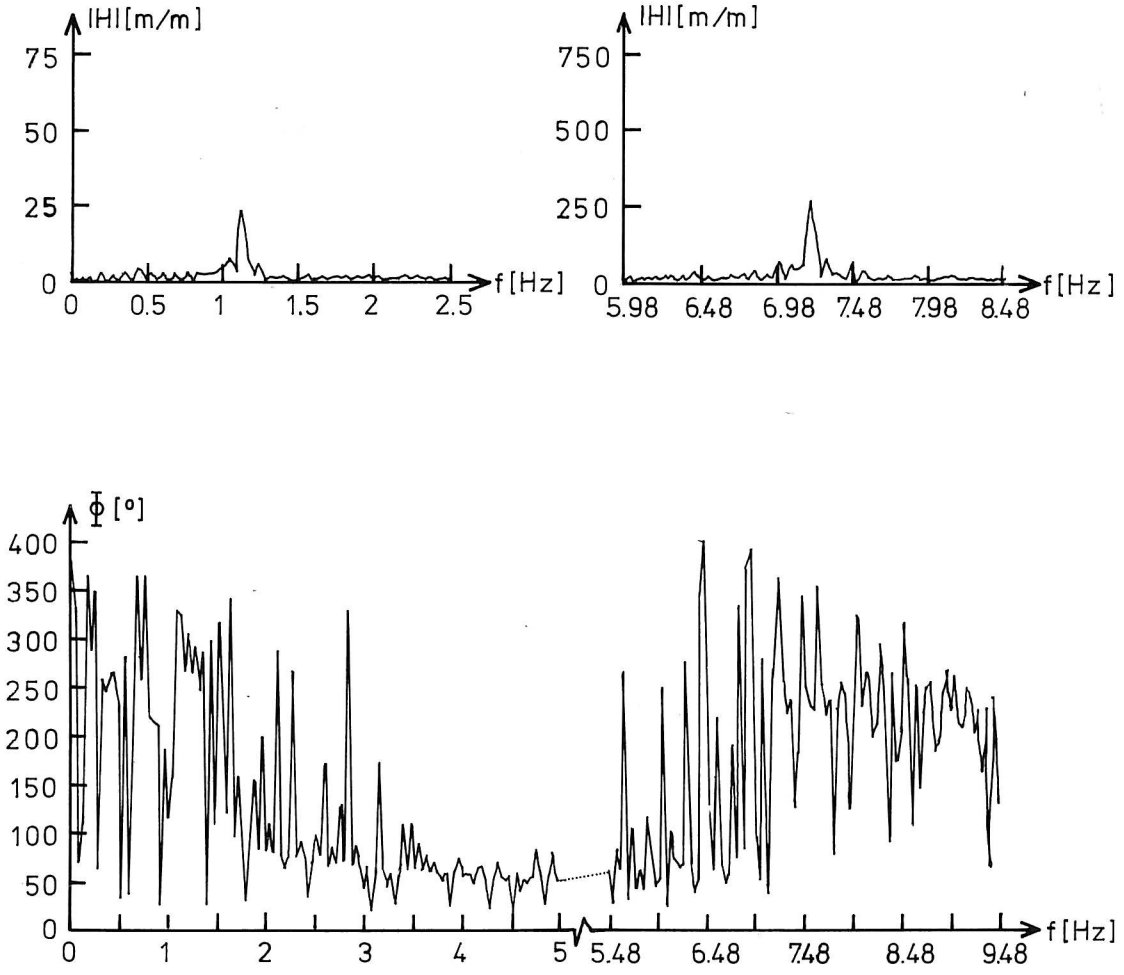

Response: Displacement of mass 2. Excitation: Periodic noise. BW=0.04 hz. Number of averages: 8. Filter cutoff frequency of the noise signal: 15 hz.

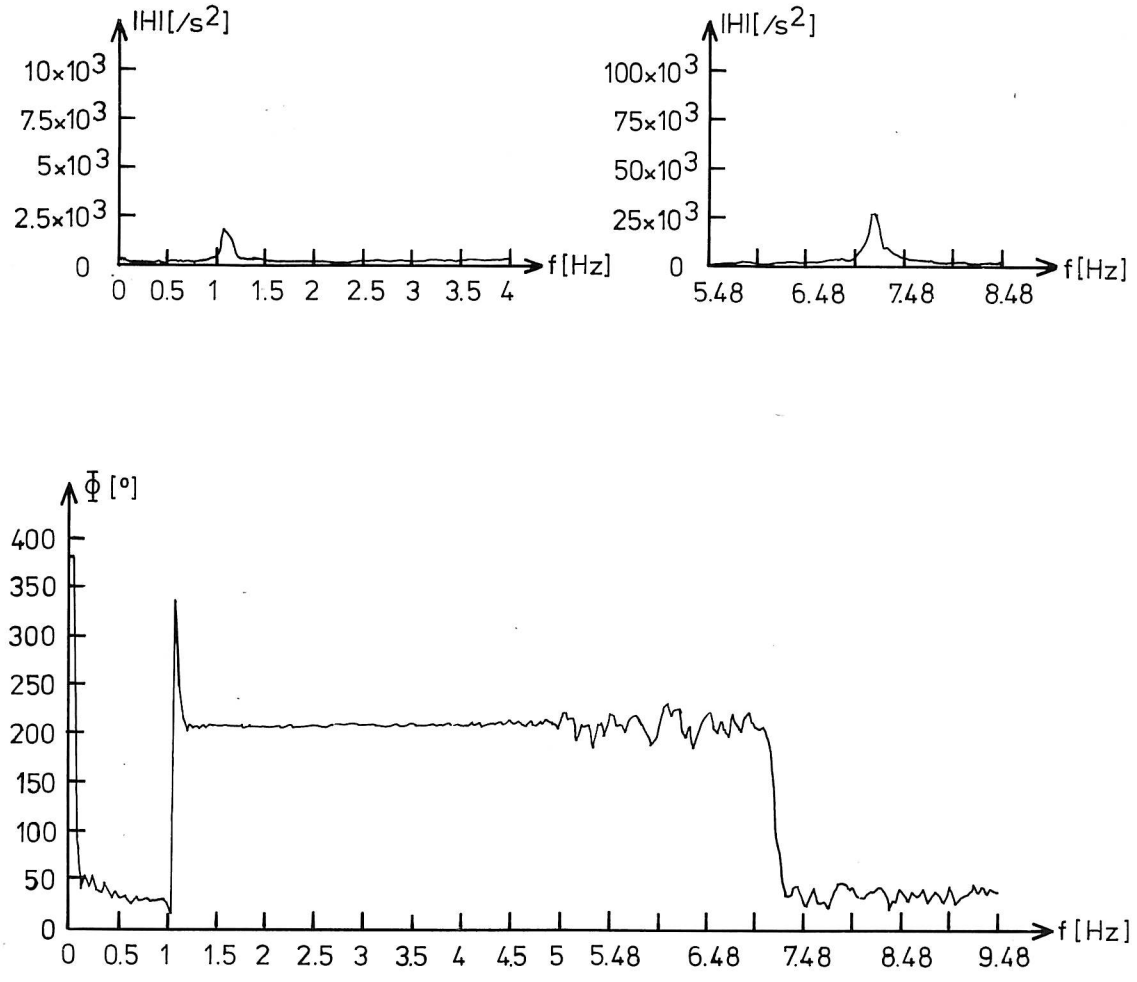

Response: Acceleration of mass 1. Excitation: White noise. BW=0.06 hz. Number of averages: 16. Filter cutoff frequency of the noise signal: 15 hz.

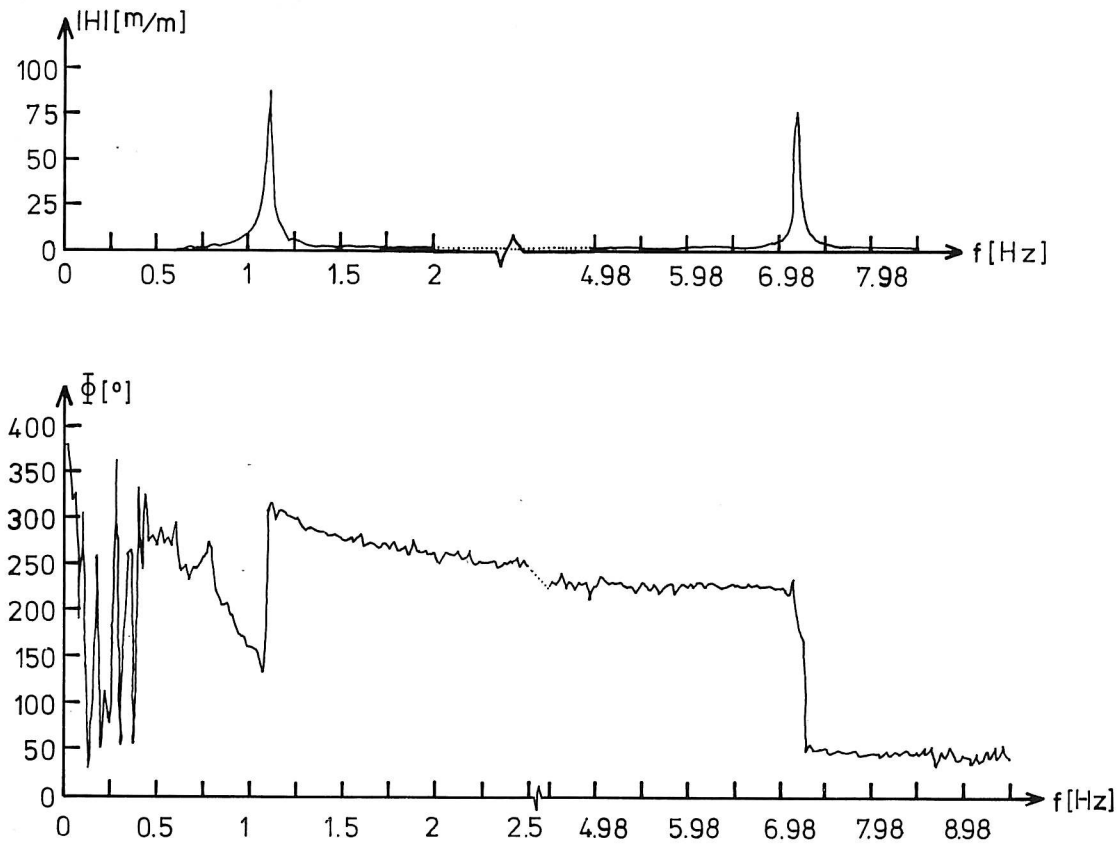

Resonse: Displacement of mass 1. Excitation: White noise. BW=0.03/0.06 hz. Number of average: 8. Filter cutoff frequency of the noise signal: 15 hz.

The FRACTURE AND DYNAMICS papers are issued for early dissemination of research results from the Structural Fracture and Dynamics Group at the Institute of Building Technology and Structural Engineering, University of Aalborg. These papers are generally submitted to scientific meetings, conferences or journals and should therefore not be widely distributed. Whenever possible reference should be given to the final publications (proceedings, journals, etc.) and not to the Fracture and Dynamics papers.

FRACTURE AND DYNAMICS PAPERS

PAPER NO. 1: J. D. Sørensen & Rune Brincker: *Simulation of Stochastic Loads for Fatigue Experiments.* ISSN 0902-7513 R8717.

PAPER NO. 2: R. Brincker & J. D. Sørensen: *High-Speed Stochastic Fatigue Testing.* ISSN 0902-7513 R8809.

PAPER NO. 3: J. D. Sørensen: *PSSGP: Program for Simulation of Stationary Gaussian Processes.* ISSN 0902-7513 R8810.

PAPER NO. 4: Jakob Laigaard Jensen: *Dynamic Analysis of a Monopile Model.* ISSN 0902-7513 R8824.

INSTITUTE OF BUILDING TECHNOLOGY AND STRUCTURAL ENGINEERING
THE UNIVERSITY OF AALBORG
SOHNGAARDSHOLMSVEJ 57, DK 9000 AALBORG
TELEPHONE: Int. + 45 - 8 - 14 23 33